Experimental Cell Research 380 (2019) 216–233

Contents lists available at ScienceDirect

Experimental Cell Research

journal homepage: www.elsevier.com/locate/yexcr

Modelling the neuropathology of lysosomal storage disorders through disease-specific human induced pluripotent stem cells

Julianna Kobolák[a,2], Kinga Molnár[b,2], Eszter Varga[a,3], István Bock[a], Bálint Jezsó[b], Annamária Téglási[a], Shuling Zhou[a,c], Maria Lo Giudice[a], Marianne Hoogeveen-Westerveld[d], WWM Pim Pijnappel[d], Phetcharat Phanthong[a,e,1], Norbert Varga[f], Narisorn Kitiyanant[e], Kristine Freude[c], Hideyuki Nakanishi[g], Lajos László[b], Poul Hyttel[c], András Dinnyés[a,h,*]

[a] BioTalentum Ltd., Gödöllő, 2100, Hungary
[b] Department of Anatomy, Cell and Developmental Biology, Eötvös Loránd University, Budapest, 1117, Hungary
[c] Department of Veterinary Clinical and Animal Sciences, Faculty of Health and Medical Sciences, University of Copenhagen, 1870, Copenhagen, Denmark
[d] Department of Clinical Genetics, Erasmus MC Rotterdam, 3015 CN, Rotterdam, the Netherlands
[e] Institute of Molecular Biosciences, Mahidol University, Bangkok, 73170, Thailand
[f] Department of Metabolic Diseases, Heim Pál Children's Hospital, Budapest, 1089, Hungary
[g] Department of Macromolecular Science and Engineering, Graduate School of Science and Technology, Kyoto Institute of Technology, Matsugasaki, Kyoto, 606-8585, Japan
[h] Molecular Animal Biotechnology Laboratory, Szent István University, Gödöllő, 2101, Hungary

Keywords:
Mucopolysaccharidosis II
iPSC
Neuronal
Storage vacuoles
Endosomal-lysosomal system
Autophagy

A B S T R A C T

Mucopolysaccharidosis II (MPS II) is a lysosomal storage disorder (LSD), caused by iduronate 2-sulphatase (IDS) enzyme dysfunction. The neuropathology of the disease is not well understood, although the neural symptoms are currently incurable. MPS II-patient derived iPSC lines were established and differentiated to neuronal lineage. The disease phenotype was confirmed by IDS enzyme and glycosaminoglycan assay. MPS II neuronal precursor cells (NPCs) showed significantly decreased self-renewal capacity, while their cortical neuronal differentiation potential was not affected. Major structural alterations in the ER and Golgi complex, accumulation of storage vacuoles, and increased apoptosis were observed both at protein expression and ultrastructural level in the MPS II neuronal cells, which was more pronounced in GFAP + astrocytes, with increased LAMP2 expression but unchanged in their RAB7 compartment. Based on these finding we hypothesize that lysosomal membrane protein (LMP) carrier vesicles have an initiating role in the formation of storage vacuoles leading to

Abbreviations: AQP4, Aquaporin-4; AMPK, AMP-activated protein kinase; BBB, blood-brain barrier; bFGF, basic Fibroblast Growth Factor; BSA, bovine serum albumin; CATD, Cathepsin D; CNS, Central Nervous System; CSF, cerebrospinal fluid; Ctrl, Control; CXC, cytochrome c; DAPI, 4′,6-diamidino-2-phenylindole; DNA, deoxyribonucleic acid; ECM, extracellular matrix; EEA1, early endosome antigen 1; EGF, Epidermal Growth Factor; ELS, endosomal-lysosomal system; ER, endoplasmic reticulum; ERT, enzyme replacement therapy; FACS, Fluorescence activated cell sorting; GAG, glycosaminoglycan; GAPDH, Glyceraldehyde 3-phosphate dehydrogenase; GFAP, Glial fibrillary acidic protein; GM130, alias Golgi Matrix Protein GM130; new name GOLGA2 GRP78, Endoplasmic reticulum chaperone BiP protein, also known as Glucose-Regulated Protein 78 kDa; hiPSC, human induced Pluripotent Stem Cell; HSCT, hematopoietic stem cell transplantation; HSPG, Heparan sulphate proteoglycans; ICC, Immunocytochemistry; IDS, Iduronate 2-sulfatase; iPSC, induced Pluripotent Stem Cell; IRE1, inositol-requiring kinase 1; LAMP2, Lysosome-associated membrane protein 2; LC3, Microtubule-associated protein 1A/1B-light chain 3; LSD, lysosomal storage disease; MA, macroautophagy; MAP2, Microtubule-associated protein 2; MPS II, Mucopolysaccharidosis type II, Hunter disease; NEAA, non-essential amino acids; NF200, Neurofilament 200 kDa; NIM, Neural induction media; NMM, Neural maintenance media; mTORC1, mammalian target of rapamycin; NPC, Neuronal progenitor cell; NSC, neural stem cell; O/N, overnight; PAX6, Paired Box 6; PBMC, Peripheral Blood Mononuclear Cell; PCR, polymerase chain reaction; PFA, Paraformaldehyde; POL/L, Poly-L-ornithine and Laminin; PTC, premature termination codon; PSD95, postsynaptic density protein 95; RAB, Ras-related protein; RBFOX3, RNA Binding Fox-1 Homolog 3; RER, Rough Endoplasmic Reticulum; RNA, ribonucleic acid; RT, Room Temperature; RT-qPCR, Reverse transcription quantitative polymerase chain reaction; S100β, S100 calcium-binding protein β; SDS, Sodium dodecyl sulphate; SEM, standard error of the mean; SNV, single nucleotide variation; SOX1, SRY-Box 1; SVZ, subventricular zone; TD, terminal differentiation; TFEB, transcription factor EB; TMA, (11-Mercaptoundecyl)-N,N,N-trimethylammonium bromide; TUBB3, Tubulin Beta 3 Class III; UPR, unfolded protein response; WB, Western-blot; XBP1, X-box binding protein 1; XCI, X chromosome inactivation

* Corresponding author. BioTalentum Ltd., Aulich L. u. 26, Gödöllő, 2100, Hungary.
E-mail address: Manuscript.Dinnyes@biotalentum.hu (A. Dinnyés).
[1] Equal contribution.
[2] Present address: Sanquin Research Amsterdam, Amsterdam, The Netherlands.
[3] Present address: Faculty of Allied Health Sciences, Burapha University, Chonburi 20131, Thailand.

https://doi.org/10.1016/j.yexcr.2019.04.021
Received 17 December 2018; Received in revised form 12 April 2019; Accepted 17 April 2019
Available online 27 April 2019

impaired lysosomal function. In conclusion, a novel human MPS II disease model was established for the first time which recapitulates the *in vitro* neuropathology of the disorder, providing novel information on the disease mechanism which allows better understanding of further lysosomal storage disorders and facilitates drug testing and gene therapy approaches.

1. Introduction

One of 40 currently known lysosomal storage diseases (LSDs), Mucopolysaccharidosis type II (MPS II; also known as Hunter syndrome; OMIM 309900) is registered on ORPHANET as a rare disease [1]; its incidence rate is 1–100,000 worldwide [2] and 1 to 166,000 in Europe [3]. MPS II is an X-linked, recessive disorder that manifests almost exclusively in males, while female carriers with a mutant and a wild-type allele are usually unaffected [4,5]. The disease is caused by deficient activity of iduronate 2-sulphatase (IDS), a lysosomal enzyme involved in the first step of the degradation pathway of the heparan and dermatan sulphate proteoglycans [6]. Deficient IDS activity results in the accumulation of glycosaminoglycans (GAGs), ultimately leading to a cascade of multisystemic disease manifestations, especially in the membrane of the cells, due to their central role in the creation of the extracellular matrix (ECM) [7]. GAG fragments generated by alternative pathways are excreted in urine and other body fluids [8].

MPS II is a progressive disease characterized by musculoskeletal abnormalities (skeletal malformations, cardiac disease, stiffness and joint contractures), organomegaly (enlarged spleen and liver), pulmonary disorders, hearing loss, eye troubles and profound neurological dysfunction in ~75% of patients [9]. Patients appear healthy at birth, with detectable initial symptoms manifesting between 18 months and 4 years of age, leading to a premature death. In relation to the pathogenicity of the IDS mutation, a wide spectrum of the disorder has been described with different onset and severity [6,10,11]. The disease is diagnosed by quantification of GAG excretion in urine or blood, or in cerebrospinal fluid (CSF), but there is currently no cure and the available treatments are mostly palliative, although there are two primary treatment options. The first, allogenic hematopoietic stem cell transplantation (HSCT) can alleviate the symptoms of MPS II [12,13], reducing urinary GAG levels, stabilizing heart function (cardiac valvular regurgitation may decrease), and improving hearing, but its efficacy on cognitive function is still debated. However, a new gene-therapy approach, using ex-vivo genome editing by CRISP/Cas9 technology, introduced the lysosomal enzyme iduronidase (IDUA) to the CCR5 safe harbor locus in human CD34 $^{+}$ hematopoietic stem cells. The IDUA overexpressing cells were transplanted into an immunocompromised mouse model of MPS I, resulting in endogenous enzyme expression, correct the biochemical, visceral, musculoskeletal, and neurologic manifestations of the disease [14]. Engineering the patient's own hematopoietic cells to express the deficient enzyme properly and in that way correcting the enzyme defect and stopping the progression of the disease has great potential and could provide a new therapeutic approach for further LSDs as well [15]. The second, enzyme replacement therapy (ERT), involves the weekly intravenous administration of recombinant human IDS enzyme (*Elaprase*™; Shire Human Genetic Therapies, Inc.), and may improve growth, joint movement, respiratory function, vision, and reduce pain sense and liver/spleen enlargement [16]. A major limitation of ERT, however, is that the enzyme is not able to penetrate the blood-brain barrier (BBB), and so cannot protect against lesions of the central nervous system (CNS) or consequently against psychomotor regression that leads to severe neurodegenerative abnormalities [17,18]. Clinical trials on the delivery of the enzyme into the CSF via intrathecal administration and gene therapy approaches are ongoing. The development of alternative, more effective treatment options for MPS II requires a better understanding of its pathophysiology at the neuronal level.

An MPS II-comparable mouse model of MPS VII showed that GAG accumulation caused by β-glucuronidase deficiency did not alter the neuronal differentiation potential [19], while neural stem cells (NSCs) derived from an IDS knock-out, MPS II mouse model displayed a self-renewal capacity with a remarkably higher dependence on the culture medium mitogens, suggesting that IDS deficit could hamper normal differentiation. Indeed, during differentiation, IDS-deficient NSCs displayed an increasing and robust accumulation of lysosomal organelles that was absent in control cells [20]. Interestingly, in healthy cells both IDS expression and activity peaked at the progenitor stage leading to the speculation that IDS could prime the correct commitment of transient progenitors and/or contribute to the establishment of an extracellular environment suitable for functional differentiation and survival of mature neurons. Moreover, when different cell types were analysed, a glial cell-mediated neurodegeneration was shown to be involved as a possible pathomechanism of MPS II [21,22]. Although these results in an MPS II mouse model are important, species-specific differences appearing mainly in the CNS would require a faithful human model which is not yet available.

In this study we raised the question whether the neuronal pathomechanism of MPS II disease can be modelled in an *in vitro* system through patient-derived iPSC lines. Our goal was to establish an MPS II specific iPSC-based *in vitro* model and to examine whether it recapitulates the disease phenotype. Ultrastructural morphology of MPS II peripheral blood mononuclear cells (PBMCs), iPSC derived NPCs and terminally differentiated (TD) cortical neuronal cells were evaluated. The relationship between storage vacuoles and endosomal-lysosomal system was also investigated. Our results may explain the origin of storage vacuoles and the cellular pathomechanism of neurodegeneration, as well as suggest further research/development directions.

2. Methods

2.1. Chemicals

The chemicals were purchased from Sigma-Aldrich (St Louis, MO, USA) and all cell culture reagents from Thermo Fisher Scientific Inc. (Waltham, MA, USA), unless otherwise specified.

2.2. Cell lines

In each assay, a healthy donor-derived iPSC line (originated from a 32-years old Caucasian female) was used as control (Ctrl), which was generated by the same process as the disease-specific iPSCs (Fig. S1). The disease-specific iPSC lines of this study were established and published earlier by us: MPSII-1.3 [23], MPSII-2.5 [24], MPSII-4.1 [25], and Ctrl-M.1 [26]. Briefly, the MPSII-1.3 and MPSII-2.5 lines were generated from male donor siblings (1- and 3 years-old, respectively) carrying the same mutation (NM_000202.7(IDS):c.85C > T, p.Gln29Ter) [23,24], while Ctrl-M.1 (MPSII-mother.1) was derived from the PBMCs of their mother (39-years old), who is an unaffected carrier [26]. The MPSII-4.1 line was derived from an unrelated male patient (7-years old) with the disease, carrying a different point mutation (NM_000202.7(IDS):c.182C > T, p.Ser61Phe) as published earlier [25].

2.3. Human iPSC culture

Cells were cultured at 37 °C in a humidified atmosphere containing 5% CO_2. The iPSCs were cultured on Matrigel (BD Biosciences, Franklin Lakes, NJ, USA) with mTeSR-1 medium (Stem Cell Technologies, Vancouver, Canada), using the clump-passage system, according to the manufacturer's instructions.

2.4. Neuronal differentiation and maintenance

The iPSCs were differentiated to neuronal progenitor cells (NPCs) by the dual SMAD inhibition procedure [27], following the detailed protocol of Shi et al. [28]. In brief, until day 10 of differentiation, 10 μM SB431542, 500 ng/mL Noggin (R&D Systems, Inc., Minneapolis, MN, USA) and 5 ng/mL bFGF in neural induction medium (NIM; DMEM/F12: Neurobasal medium, supplemented with 1xN2 and 2xB27, 2 Mm glutamine, 1 × non-essential amino acid (NEAA), 100 μM β-mercaptoethanol, 5 μg/mL insulin) was used to induce the neuroectodermal lineage. Tissue culture plates were coated with poly-L-ornithine and laminin (POL/L; 0.002%/1 μg/cm^2). The forming neuronal rosette-like structures were manually picked under a sterile microscope (Olympus SZX2; Olympus Corporation, Shinjuku, Japan) and re-plated onto POL/L plates. NPCs were expanded in neural maintenance medium (NMM; DMEM-F12: Neurobasal medium, supplemented with 1xN2 and 2xB27, 2 Mm glutamine, 1xNEAA), supplemented with 10 ng/mL bFGF and 10 ng/mL EGF. NPCs were passaged when reached 100% confluence, using Accutase and single cell-seeded (50,000 cells/cm^2) for further expansion.

NPCs were terminally differentiated (TD) towards cortical neurons by harvesting the cells using Accutase and plating them on POL/L (0.002%/2 μg/cm^2) at a seeding density of 40,000 cells/cm^2 with NMM medium [28]. The medium was changed every 3–4 days for up to 5 weeks (35 days, labelled as TD35). To note, both NIM and NMM media was serum-free, no FBS was used in the cell cultures.

2.5. Immunocytochemistry (ICC) staining

The expression of neural markers was analysed using conventional ICC staining. The cells were fixed in 4% PFA (20 min, RT), permeabilized with 0.1% Triton X-100 (5 min) and blocked in 1% bovine serum albumin (BSA) containing PBS (1 h, RT). The cells were incubated with primary antibodies (O/N, 4 °C) and visualized with secondary antibodies (listed in Table S3). For nuclei counterstaining 0.2 μg/mL DAPI (20 min, RT) was used. The cells were observed under a fluorescence microscope equipped with a 3D imaging module, (AxioImager system with ApoTome, Carl Zeiss MicroImaging GmbH, Jena, Germany) controlled by AxioVision 4.8.1 Microscope software (Carl Zeiss).

2.6. Fluorescence activated cell sorting (FACS)

NPCs were collected using 0.5% trypsin to get a single cell suspension and were fixed in 4% paraformaldehyde (PFA; 20 min, RT). After fixation, the cells were permeabilized with 0.2% Triton X-100 (5 min, RT); followed by blocking with 1% BSA (15 min, RT). The cells were then incubated with the corresponding antibodies for 1 h at RT. For unconjugated primary antibodies the isotype specific secondary antibodies were used accordingly (see Table S3). To measure cell proliferation, cells were treated with ice cold 70% ethanol (20 min) and stained (20 min, RT) with FITC anti-human Ki67 antibody (Miltenyi Biotec, Bergisch Gladbach, Germany). Samples were analysed using a 'Cytomics FC 500' Flow Cytometer (Beckman Coulter). Data were analysed using FlowJo software (version 7.6.5; FlowJo, LLC).

2.7. Caspase 3/7 assay

To detect the activated Caspase-3/7 in neuronal cultures, live TD35 neurons were incubated with the CellEvent™ Caspase-3/7 Green Detection Reagent for 30 min (5 μM at 37 °C) according to the manufacturer's protocol and grown in POL/L (0.002%/2 μg/cm^2) treated 96-well plates (40,000 cells/cm^2 density). For a positive control, cell cultures were treated with 0.5 μM Staurosporine in the presence or absence of the Caspase 3/7 Inhibitor 1 (10 μM for 2 h; MERCK, Kenilworth, NJ. USA). Cell cultures were analysed using a Varioskan Flash (Thermo Fisher Scientific) microplate reader (Ex/Em: 502/530 nm).

2.8. Fluorometric IDS enzyme assay

PBMCs, iPSCs and NPCs were used in the determination of IDS enzyme activity. The homogenates were prepared by sonication, and the protein concentration was determined by the Pierce™ BCA Protein Assay Kit and measured by spectrophotometer. Iduronate-2-sulphate enzyme activity was assayed using fluorogenic substrate 4-methylumbelliferyl-α-L-iduronate-2-sulphate, according to the method described by Voznyi et al. [29].

2.9. GAG assay

Sulphated proteoglycans and glycosaminoglycans (sGAG) were quantified by using the Blyscan™ Glycosaminoglycan Assay (Biocolor Ltd., Carrickfergus, UK) following the manufacturer's instructions. NPCs or terminally differentiated neuronal cultures were grown on 6-well plates in 4 parallels for each experiment. Samples were measured with a Varioskan Flash (Thermo Fisher Scientific) microplate reader and the results were analysed using its software (SkanIt Software).

2.10. Western blot

The cell cultures were lysed with RIPA Lysis and Extraction Buffer supplemented with Halt™ Protease and Phosphatase Inhibitor Cocktail and Pierce™ Universal Nuclease for Cell Lysis (all from Thermo Fisher Scientific), sonicated and the total protein concentration determined using a Pierce BCA Protein Assay Kit. Protein samples (2–5 μg/sample) were separated on 12% SDS-polyacrylamide gels and transferred to Immun-Blot® PVDF Membrane (Bio-Rad, Hercules, CA, USA). The membranes were blocked with TBST (20 mM Tris-HCl pH 7.4, 150 mM NaCl, 0.1% Tween-20) containing 5% low-fat dried milk (1 h, RT), then incubated overnight at 4 °C with primary antibodies (Table S4). After washing with TBST, the membranes were incubated with horseradish peroxidase (HRP)-conjugated secondary antibodies 1:2000 (Sigma Aldrich) for 1 h (RT). Signals were detected with SuperSignal™ West Dura Extended Duration Substrate (Thermo Fisher Scientific) by KODAK Gel Logic 1500 Imaging System and Kodak MI SE imaging software. Densitometry measurement of protein bands intensity was carried out using Image Studio™ Lite software (LI-COR; LI-COR Biosciences, Lincoln, Nebraska, USA).

2.11. Nanogold particle uptake

NPCs were cultured in the presence of 0.5 μ M TMA (11-Mercaptoundecyl)-N,N,N-trimethylammonium bromide) 5 nm nanogold particles [30,31] in NMM media supplemented with EGF and bFGF for 12 and 24 h, then fixed and handled as detailed in electron microscopy section [32–34].

2.12. Electron microscopy

Frozen PBMCs were thawed, centrifuged in chilled PBS buffer, then 30% BSA was applied to 'glue' the cells and the pellets were fixed with 5% glutaraldehyde in 0.1 M cacodylate buffer (pH 7.4; 1 h, RT). NPCs were detached from the surface by Dispase treatment and pelleted by centrifugation, while terminally differentiated cortical neurons grown on coverslips in 24-well tissue culture plates were fixed with solution containing 3.2% PFA, 0.2% glutaraldehyde, 1% sucrose, 40 mM $CaCl_2$ in 0.1 M cacodylate buffer. Samples for ultrastructural analysis were post-fixed with 1% ferrocyanide-reduced osmium tetroxide [35], dehydrated using a graded ethanol series, then embedded in Spurr low viscosity epoxy resin medium. Ultrathin sections were collected on Formvar (Agar Sci., Essex, UK) coated copper slot grids, counterstained with uranyl acetate and Reynolds's lead citrate, and examined on a JEOL JEM 1011 transmission electron microscope equipped with a Morada 11-megapixel camera (Olympus) using iTEM software.

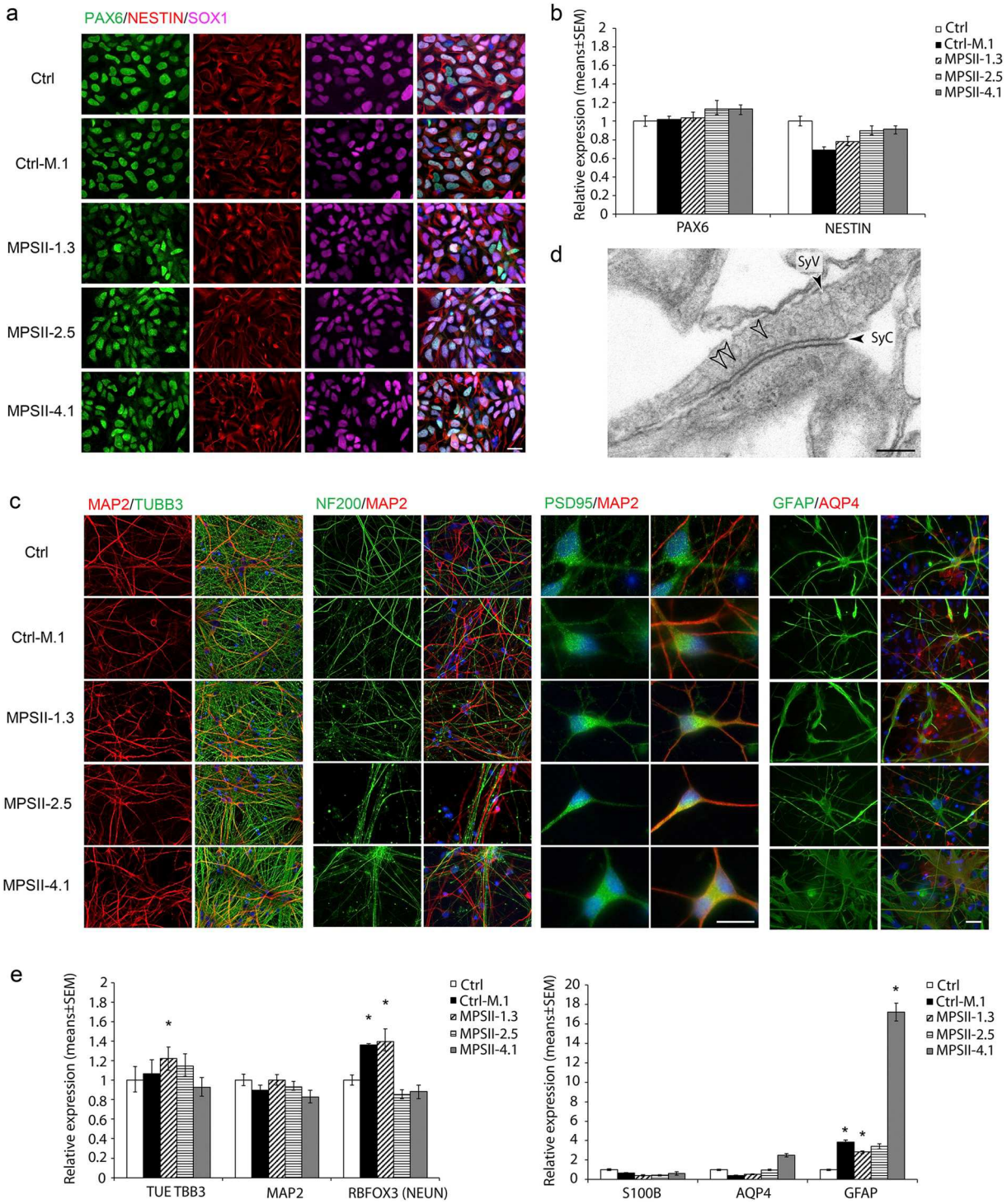

Fig. 1. Comparison of healthy and MPS II iPSC derived NPC and TD35 neuronal cultures. a) Neuronal precursor cells (NPCs) were differentiated from iPSC lines stained with PAX6 (green) NESTIN (red) and SOX1 (magenta) antibodies. Nuclei were counterstained with DAPI (in blue). Scale bar: 20 μm; **b**) RT-qPCR analysis of PAX6 and NESTIN transcripts showed similar expression in early passage NPCs. Values are expressed as relative expression normalized to the Ctrl, set as 1. Data are presented as mean ± SEM (n = 3). *p < 0.05; **c**) TD35 neuronal cultures were characterized by immunocytochemical staining TUBB3 (green)/MAP2 (red), NF200 (green)/MAP2 (red), PSD95 (green)/MAP2 (red) and GFAP (green)/AQP4 (red). Nuclei were counterstained with DAPI (in blue). Scale bar: 20 μm; **d**) Representative ultrastructural morphology picture of an active synapse in Ctrl TD35 neurons. Symmetric synapse with accumulating synaptic vesicles (SyV) in presynaptic terminal and electron-dense material in synaptic cleft (SyC). Active zone is indicated by docking synaptic vesicles (white arrowheads) Scale bar: 100 nm; **e**) Expression of neuronal marker genes in patient and control iPSCs-derived TD35 neuronal cultures evaluated by RT-qPCR. Values are expressed as relative expression normalized to the Ctrl, set as 1. Note the different values of the y-axis. Data are presented as mean ± SEM (n = 3). *p < 0.05.

For samples destined for immunogold labelling, an LRG embedding procedure with a progressive temperature decrease (to preserve membranes and antigenicity of proteins) was used (modification of the method described by Berryman and Rodewall) [36].

2.13. Post-embedding immunolabeling of ultrathin sections

Ultrathin sections (60–80 nm) were collected on Formvar coated 200 mesh nickel grids. Antigen retrieval was achieved by exposure to 5% hydrogen peroxide (5 min) and incubation in 1% sodium borohydride and 50 mM glycine dissolved in TBS (10 min) before blocking (3% milk powder and 1% BSA in TBS, 30 min). The sections were incubated overnight with primary antibodies diluted in TBS supplemented with 1.5% milk powder and 0.5% BSA (Table S5). All primary antisera were polyclonal and developed in the rabbit against human peptides or peptide sequences. The sections were then incubated for 6 h with anti-rabbit 10 nm gold-conjugated IgG secondary antibody (1:100; dissolved in TBS supplemented with 1% BSA) before being counterstained and examined as described above.

2.14. RT-qPCR analysis

Total RNA was isolated from NPC and neuronal cultures (TD35) using the RNeasy Plus Mini Kit (Qiagen, Hilden, Germany). For the reverse transcription, 600 ng isolated RNA was used with the Maxima First Strand cDNA Synthesis Kit for RT-qPCR with dsDNase (Thermo Fisher Scientific) according to the manufacturer's instructions.

Primers were optimized using two-fold serial dilution standard curves. *GAPDH* was used as the reference gene (Table S6). Each real-time PCR reaction contained 5 ng RNA equivalent cDNA template, 400 nM of each primer and 50% SYBR Green JumpStart Taq ReadyMix (Sigma Aldrich) in a total volume of 15 µL. PCR reactions were set up using a QIAgility liquid handling robot and were performed on a Rotor-Gene Q cycler (Qiagen). The cycling parameters were: 94 °C for 3 min initial denaturation followed by 40 cycles of 95 °C for 5 s, 60 °C for 15 s and 72 °C for 30 s. Melting curve analysis and agarose gel electrophoresis confirmed the specificity of the primers and the absence of gDNA contamination. Data of three replicates were analysed for each gene, using the Relative Expression Software Tool 2008 V2.0.7 [37].

2.15. XBP1-assay of endoplasmic reticulum stress

Upon accumulation of unfolded proteins in the endoplasmic reticulum (ER), a 26-nucleotide fragment from the X-box binding protein 1 mRNA (XBP1(U)) is removed with a special splicing mechanism [38]. This shorter mRNA (XBP1(S)) is a frequently used marker of ER-stress. To study the expression of XBP1(S), previously described primers [39] were used. As positive control, Ctrl iPSC was treated with 1 µM Tunicamycin to induce ER-stress. New RT-PCR primers were also designed to amplify both the un-spliced and the spliced variants of the XBP1 (Table S6). PCR reactions were performed using Phusion Hot Start II High-Fidelity DNA Polymerase and 20 ng of the cDNA samples. The PCR products were visualized on 2% agarose gels.

2.16. Statistical analysis

All results were analysed using Prism 5 (GraphPad Software, La Jolla, CA, USA) and Microsoft Office 2010 (Microsoft, Redmond, WA, USA) software. All data on the graphs represent the average of the triplicate measurements (n = 3). The "n" value corresponds to the number of replicates for each cell line. Analysis of data is presented as the mean ± SEM. Dunnett's method was used to compare the individual groups with control subjects. In all cases, significance was noted at $p < 0.05$.

3. Results

3.1. Patient iPSC lines

In this study two families were sampled where infants were diagnosed with MPS II disorder. One family with two male infants (MPSII-1.3 and MPSII-2.5) and their asymptomatic mother (Ctrl-M.1) were involved, all carrying a pathogenic mutation of the iduronate 2-sulfatase gene (NM_000202.7(IDS):c.85C > T). This single nucleotide variation (SNV) results in a premature termination codon in the iduronate 2-sulfatase gene. From another family one male infant (MPSII-4.1) with a missense mutation (NM_000202.7(IDS):c.182C > T) causing MPS II symptoms was involved. The sampling, genetic reprogramming and characterisation of the iPSC lines were detailed and published elsewhere [23–26]. In addition, a sample of a healthy female was used as non-linked control (Ctrl; Fig. S1). At the time of the sampling, the MPSII-2.5 and MPSII-4.1 patients were receiving ERT on a regular basis, with the last ERT performed one week before blood sampling.

3.2. Neuronal differentiation ability of iPSCs revealed an in vitro cellular disease model

Our aim was to investigate the neuronal phenotype and pathomechanism of the MPS II disease *in vitro* in a cell-based model. PBMCs were reprogrammed into iPSC lines and their pluripotency was verified as previously published [23–26]. Hence, all iPSC lines were differentiated into the neuronal lineage and NPC and TD stages were evaluated. First, NPC stage was analysed based on the expression of major NPC markers (NESTIN, SOX1 (SRY- Box 1) and PAX6 (Paired Box 6) using ICC staining, which did not reveal a marked difference between the healthy and diseased cell lines in early passages (up to passage 7–8) (Fig. 1a). In parallel, RT-qPCR experiments were performed on early passage NPCs that showed similar expression levels of PAX6 and NESTIN (Fig. 1b).

Next, the NPCs were terminally differentiated into mature neurons and their characteristics were analysed after 5 weeks of culture (TD35). Terminal differentiation resulted in the formation of neuronal networks, where both healthy and diseased cells were positive for Tubulin Beta 3 Class III (TUBB3), the dendritic marker Microtubule-associated protein 2 (MAP2), and Neurofilament 200 kDa (NF200). Neurons expressed postsynaptic density protein 95 (PSD95) which indicated the formation of synapses (Fig. 1c) in all cell lines. This was confirmed by electron microscopy, where active synapses were identified (Fig. 1d). During neuronal differentiation, astrocytes also appeared showing Glial fibrillary acidic protein (GFAP) and Aquaporin-4 (AQP4) expression (Fig. 1c) regardless of cell line.

Transcriptomic analysis showed that neuronal marker genes TUBB3 and MAP2 were highly expressed in all TD35 neuronal cultures. The terminal marker RNA Binding Fox-1 Homolog 3 (RBFOX3, known as NEUN), the astrocyte-related AQP4, S100 calcium-binding protein β (S100β) and GFAP were robustly expressed in TD35, highlighting the presence of a glial lineage in all neuronal cultures (Fig. 1e). The highest GFAP expression was observed in MPSII-4.1 neuronal cultures which was correlated with the number of GFAP + astrocytes detected in the ICC experiments.

In summary, dual SMAD inhibition-driven neuronal induction resulted in the formation of MPS II NPC populations with normal proliferative capacity in early passages and supported their neuronal and astrocyte differentiation with a transcript- and protein expression pattern similar to the control line. Until TD35 stage, a mature, synaptically active neuronal population was successfully differentiated from all genotypes.

3.3. Decreased proliferation capacity of MPS II NPC cultures

When NPC populations were maintained over 8 passages, the proliferation of MPS II NPC cultures slowed or even stopped and 15–30% of the cells significantly ($p < 0.05$) decreased their PAX6 and SOX1 protein expression in the presence of bFGF and EGF. In contrast, control NPCs

proliferated for up to 12 passages with less reduction in their competence. This observation was confirmed by FACS analysis, using cell proliferation marker Ki-67 (MKI67), and early NPC markers PAX6 and SOX1 (Fig. 2a). Moreover, morphological alterations were also observed in these cultures: MPS II NPCs started to grow neurites and differentiate into neurons despite the presence of the mitogens (Fig. 2b).

The capacity for self-renewal/proliferation associated with the multipotent progenitor state was limited in the MPS II NPC cultures, and might be related to the disease pathology.

3.4. Patient derived neuronal cells showed increased apoptosis

When MAP2 and TUBB3 ICC staining were compared more thoroughly in TD35 samples, a stippled staining pattern was identified in some of the

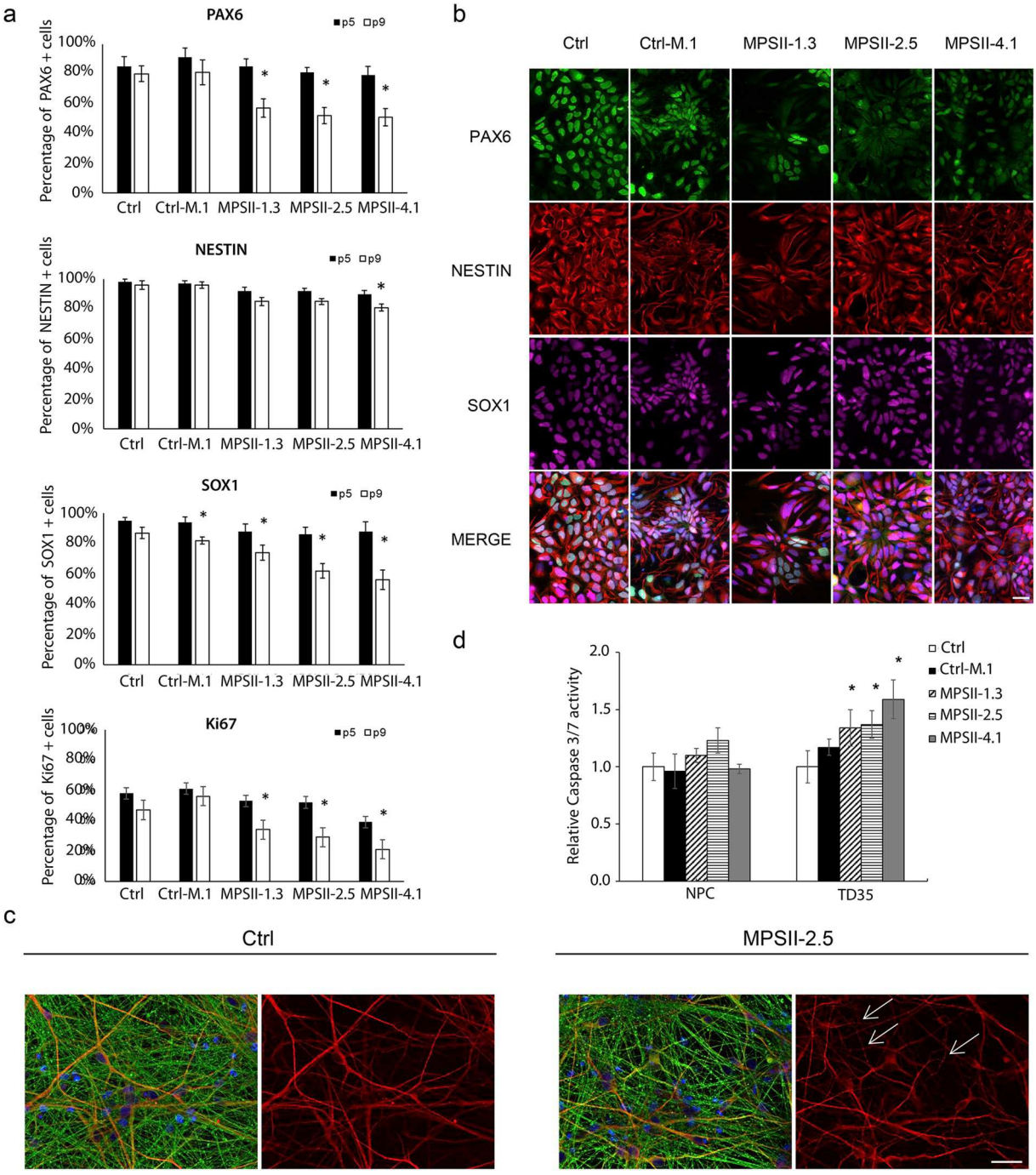

Fig. 2. Characterisation of neuronal precursor cells. **a**) Early (p5) and late (p9) NPC populations were stained and compared by flow cytometry for neuronal stem cell (PAX6, SOX1, NESTIN) and cell division (Ki67) markers. With increasing passage number, the proportions of PAX6 and SOX1 positive cells were significantly decreased in MPSII patient derived cells. This was in accordance with the decreasing number of dividing cells, labelled with Ki67. Data are presented as percentage of positive cells ± SEM (n = 3). *p < 0.05; **b**) Late passage (p9) NPCs were immunostained against PAX6 (green), NESTIN (red) and SOX1 (magenta), showing a decreased neuronal stem cell marker expression. Nuclei were counterstained with DAPI (in blue). Scale bar: 20 μm. **c**) MAP2 and TUBB3 immunostaining showed a stippled staining pattern in the neurites of MPS II patient-derived TD35 neuronal cultures. **d**) Fluorescent Caspase 3/7 assay revealed increased Caspase 3/7 activation in MPS II TD35 neuronal cells, but not in the NPCs. Average activity data (n = 3; ± SEM) is presented relative to Ctrl samples which was considered as 1. *p < 0.05.

dendrites in the patients' samples, suggesting that cell death had occurred (Fig. 2c). Therefore, a Caspase 3/7 activity assay was performed to study if the disturbed expression of MAP2 and TUBB3 was linked to apoptotic events in the diseased neurons. Patients' TD35 samples showed significantly increased expression levels of Caspase3/7 ($p < 0.05$) compared to the Ctrl (considered as 1), while the carrier cell line Ctrl-M.1 did not differ significantly from the Ctrl ($p > 0.05$; Fig. 2d). We also investigated the Caspase 3/7 activity in NPC stage cells but did not detect any significant difference between healthy and diseased samples (Fig. 2d). Our results thus demonstrated a significantly increased apoptotic activity in all three patient-derived TD35 neuronal cultures compared to the Ctrl and the carrier Ctrl-M.1 cell cultures, suggesting a disease-related phenotype in the mature neurons.

Next, the expression of Caspase-9 (CASP9), both the pro-caspase (47 kDa) and cleaved forms (37 kDa and 35 kDa) were detected in the TD35 cell cultures using Wester-blot. Results showed non-significant difference in the ratio of cleaved CASP9 compared to the controls (Ctrl and Ctrl-M.1) (Fig. S2).

3.5. IDS enzyme activity is significantly decreased in MPS II patients' cells

The presence of the pathogenic IDS mutations in the iPSC lines was previously validated by Sanger sequencing [23,26]. When the IDS activity was measured by 4-methylumbelliferyl-α-L-iduronate-2-sulphate fluorescent assay [40] in cell lysates of the control, carrier and patient iPSC lines, no IDS enzyme activity could be detected in the PBMC, iPSC or NPC stage of MPS II samples, whilst Ctrl and Ctrl-M.1 carrier cells showed normal IDS activity in all cell types (Fig. 3a). Different IDS enzyme activity was measured among the different cell types as expected. The assay confirmed that the studied mutations of the three patients resulted in the overall loss of the IDS enzyme activity in the primary cells, the PBMCs, while *in vitro* cultivation, genetic reprogramming or neuronal differentiation did not restore the enzyme activity.

3.6. GAG accumulation showed correlation with LAMP2 expression in patient-derived neuronal cells

The IDS enzyme deficiency causes a progressive accumulation of GAG in the cells of MPS II patients [41]. Therefore, we investigated whether this phenotype could also be observed in our *in vitro* cellular model. The total GAG levels of both the NPCs and the terminally differentiated neurons were measured, and all three MPS II NPC cultures showed lower total GAG levels ($p < 0.05$) compared to the control and carrier (Ctrl-M.1) cell lines (Fig. 3b). Marked GAG accumulation was detected in the neurons of MPSII-1.3 and MPSII-2.5 patients ($p < 0.05$), while MPSII-4.1 and Ctrl-M.1 neurons did not differ significantly from the Ctrl cell line ($p < 0.05$; Fig. 3b).

Accumulation of lysosomes was detectable when lysosome-associated membrane glycoprotein 2 (LAMP2) ICC staining was performed on the neuronal cultures (Fig. 3c). We detected a cell type specific difference in the TD35 patient's samples, with many more LAMP2+ vacuoles in GFAP + astrocytes than in MAP2+ neurons (Fig. 3c). Western-blot analysis to quantify the amount of LAMP2 revealed increased LAMP2 expression in MPS II NPCs (Fig. 3d). However, in the TD35 neuronal cultures, significant differences ($p < 0.05$) were detected only in MPSII-4.1 cell line, where the GFAP expression was found to be the most robust by RT-qPCR and ICC (Fig. 1c and d).

Next, we investigated if transcription factor EB (TFEB) expression and subcellular localisation is changed in the affected cells. When TFEB ICC was performed on NPCs, patient derived NPCs showed increased TFEB signal in their nuclei more often than the controls (Ctrl, Ctrl-M.1), which is a sign of the nuclear transport of the protein (Fig. 3e). Western-blot experiments did not reveal significant difference in the overall amount of the TFEB protein in the NPC samples (*data not shown*). The TD35 neuronal cultures gave similar results to the NPC cultures, when TFEB localisation was investigated (Fig. 3e).

Together these data suggest the accumulation of both GAGs and LAMP2+ vacuoles in MPS II iPSC derived neuronal cells, with differences in abundance between dividing NPCs and terminally differentiated, post-mitotic neuronal cultures, particularly GFAP + astrocytes.

3.7. Storage vacuole accumulation was prominent in patients' cells

Next, we questioned whether the cytopathological hallmark of MPS II affected cells, the accumulation of storage vacuoles, could be detected at the ultrastructural level in the MPS II iPSC derived neuronal cells. Electron microscopy techniques revealed massive storage vesicle accumulation in all MPS II NPC cultures (Fig. 4a–e). Vacuoles with characteristic morphology were classified into four groups (primary (Pr), globular (Glo), multilamellar (ML) and sequestered (Sq) type) on the basis of previous studies [42,43] as presented in Fig. S3. The frequency of different vacuole types was determined by semiquantitative scoring (Table S1).

Unexpectedly, storage vacuoles were also detectable in the healthy carrier Ctrl-M.1 sample (Fig. 4b and c), although the number of affected cells was much lower in this culture than in patients' samples. The Pr vacuole was the most abundant type in all patients' NPCs, with the other three types (Glo, ML and Sq vacuoles) also well represented (Fig. 4d and e; Fig. S3; Table S1).

All types of storage vacuoles were also detectable in the carrier Ctrl-M.1 and MPS II patients' TD35 neuronal cultures. Again, the Pr vacuole was the most frequent type in all MPS II TD35 samples (Fig. 4g–i) while the Sq type (Fig. S4) was rarer in the MPSII-2.5 and the MPSII-4.1 than in the MPSII-1.3 TD35 cultures (Table S1). It should be noted that autophagosomes were found rarely in all MPS II cultures.

Storage vacuoles were also detected in the PBMCs of the MPS II patients (Fig. S5) proving their original existence in the diseased individuals [44,45] and their independence from the genetic reprogramming and/or *in vitro* cultivation. In conclusion, the Pr storage vacuoles were most enriched in the MPS II and carrier Ctrl-M.1 NPCs and TD35 cultures, while other vacuole types accumulated with varying incidence.

3.8. The involvement of late endosomal-lysosomal system in the neuronal pathomechanism of MPS II

We performed immunogold labelling on NPCs to evaluate the involvement of storage vacuoles in the endosomal-lysosomal system (ELS), studying RAB5 as an early endosomal marker, RAB7 as a late endosomal marker, Cathepsin D (CATD) and LAMP2 as lysosomal markers and RAB2 as a Golgi-derived membrane marker. RAB5 immunopositivity was observed on plasma membrane, small membrane pits, early endosomal elements, internal vesicles and multilamellar figures of MPS II NPCs (Fig. 5a–c). RAB7 and CATD antisera gave no reaction on Pr vacuoles (Fig. 5e, i-j), although they labelled ML, larger multivesicular and Sq types of vacuoles (Fig. 5f, i-j). Analysis of RAB2 labelling revealed positive cisterns and small cytoplasmic vesicles in the Golgi area, on limiting and inner membranes of storage vesicles (Fig. S5). These observations raise the possibility of a functional connection between storage vacuoles and the Golgi complex. LAMP2 was detected on Pr (Fig. 5h), Glo, ML and Sq type vacuoles as well (Figs. S6a–b). In addition, we found gold particles on several small cytoplasmic vesicles, some of which seemed to fuse with other vesicles, for example with storage vacuoles (Fig. 5g and h).

During the evaluation of ultrathin sections, we noticed the clearance of undigested material by exocytosis in both NPC and TD cultures. We found that all types of storage vacuoles were able to fuse with plasma membrane independent of their content. Exocytosed vesicles detected by immunocytochemical experiments were positive for RAB7, CATD, LAMP2 but not RAB5 (Fig. S7). The results of immunogold labelling are summarized in Table S2.

Next, we performed immunoblot experiments to compare protein levels in NPCs and TD35 cultures. Western blot experiments for RAB5

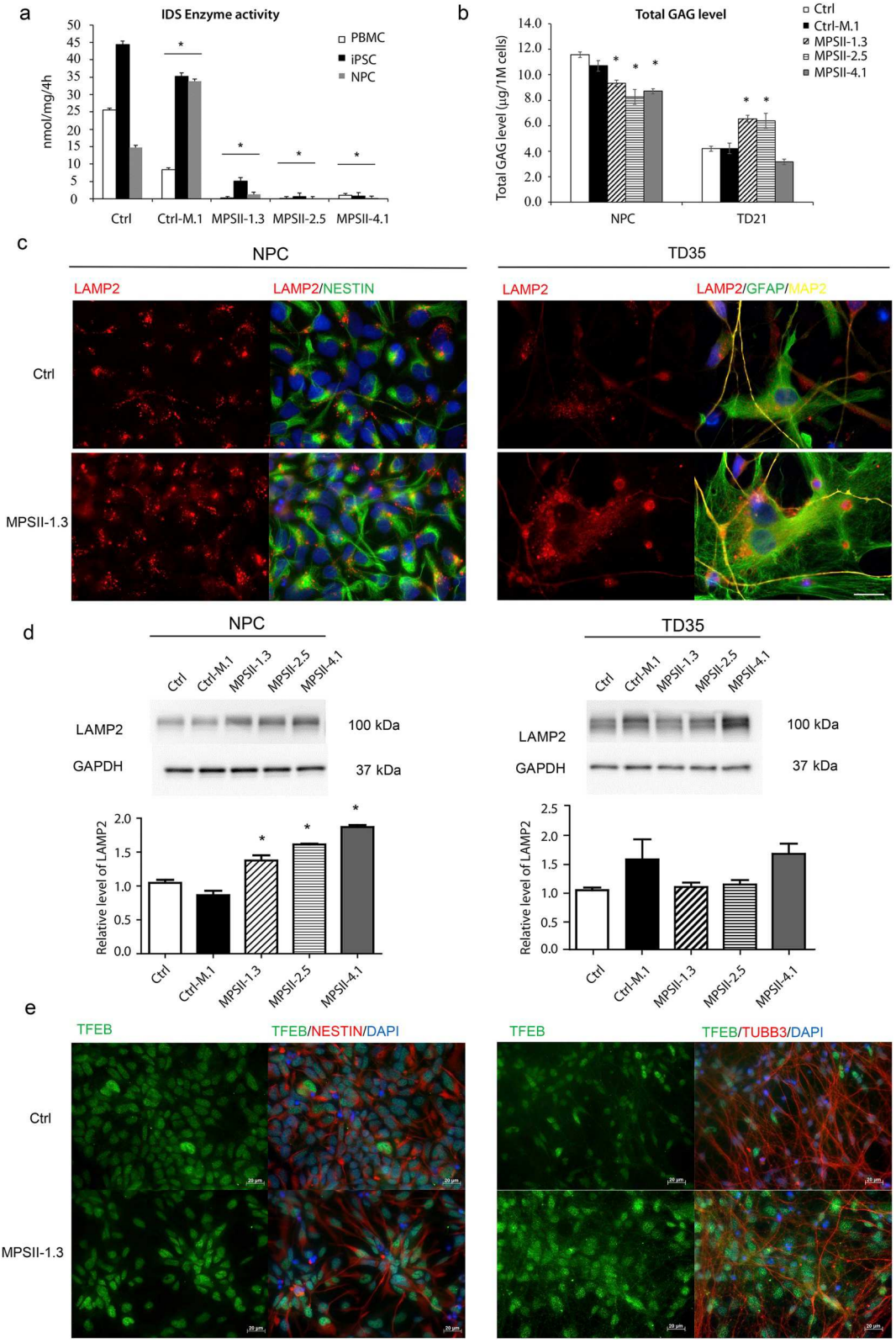

Fig. 3. IDS enzyme activity, total GAGs levels and LAMP2 expression of MPS II neuronal cells. a) IDS enzyme activity measured in the lysate of patients' mononuclear blood cells (PBMCs), genetically reprogrammed hiPSCs and in their derived NPCs, by 4MU fluorescent assay. Enzyme activity significantly decreased or dropped to zero in patient samples, in all cell types (MPSII-1.3; MPSII-2.5 and MPSII-4.1), while the enzyme activity was in the normal range in the control and decreased in the carrier mother (Ctrl-M.1) cells. Data are presented as mean ± SEM (n = 3). *p < 0.05; **b**) Total GAGs were determined in NPC and neuronal cultures. Diagrams shows the total GAG levels in µg normalized to 1×10^6 cells. Data are presented as mean ± SEM (n = 4). *p < 0.05; **c**) Representative LAMP2 immunostaining of NPCs and TD35 neuronal cultures combined with NESTIN or MAP2 and GFAP respectively, which showed increased LAMP2 positive vacuole accumulation in MPS II patient's (MPSII-1.3) neuronal cells, with more prominent accumulation in GFAP positive astrocytes. Scale bar: 10 µm; **d**) Western blot analysis confirmed the protein expression of LAMP2 in NPC and TD35 cell lysates. Signals were normalized to GAPDH, data are presented as mean ± SEM (n = 3). Dunnett's test was performed to evaluate the significance of groups compared with the control (Ctrl). *p < 0.05). **e**) Representative TFEB immunostaining of NPCs co-labelled with NESTIN, and TD35 neuronal cultures co-labelled with TUBB3, showing the dominant nuclear localisation of TFEB in MPS II cells. Scale bar: 20 µm.

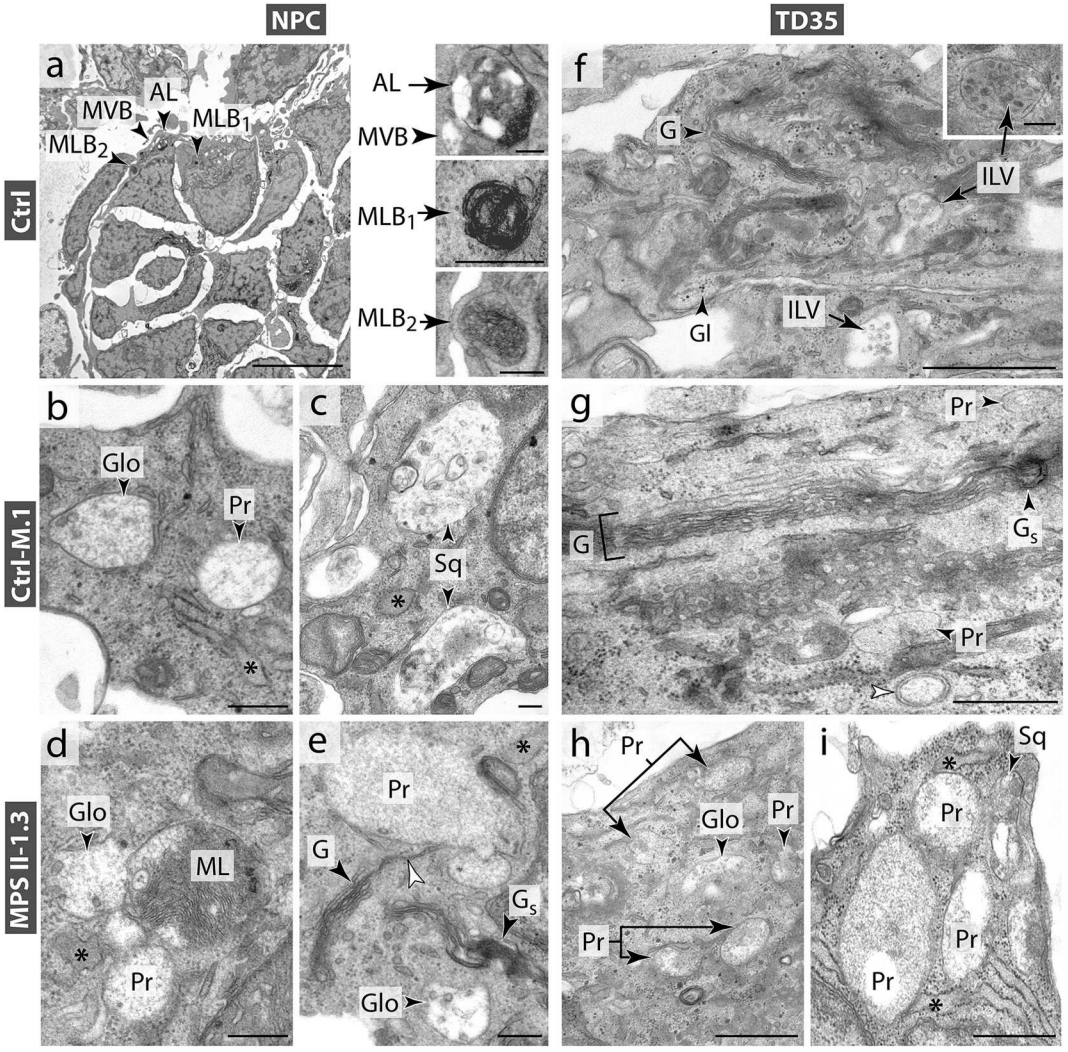

Fig. 4. Ultrastructure of NPC and TD35 neuronal cultures in MPS II disease. **a**) Ultrastructure of Ctrl NPCs by EM. Overview of the culture with intact cells attaching to each other. Insets of panel a: autolysosome (AL), multivesicular body (MVB) and two types of multilamellar bodies (MLB1, MLB2) are visible in cells. **b-e**) Storage vacuoles in Ctrl-M.1 and MPSII-1.3 NPCs: primary (Pr, panel b, d, e), globular (Glo, panel b, d, e), multilamellar (ML, panel d) and sequestered (Sq, panel c) types. Golgi stacks with short cisterns (G) and skein-like deformation (Gs) are shown in panel e. Primary vacuole seems to be in connection with cistern-like element in panel e (white arrowheads). **f**) Astrocytes in healthy Ctrl TD35 culture show glycogen granules (Gl), Golgi area with Golgi ribbon formed by three Golgi stacks (G) and endosomal elements enclosing internal vesicles (ILV) can be seen. Inset demonstrates a multivesicular body filled with dense intraluminal vesicles (ILV). **g**) Neuron of Ctrl-M.1 TD35 culture contains primary vesicles (Pr) at well-developed Golgi ribbon (G). Right Golgi stack shows skein-like deformation (Gs). White arrowhead indicates a phagosome. h-i) Storage vacuoles in MPSII-1.3 TD35 culture. Primary (Pr, panel **h, i**), globular (Glo, panel h) and sequestered (Sq, panel i) storage vacuoles can be detected in astrocytes (panel h) and a neuron (panel i). Swollen RER cisterns (black asterisk in panel b, c, d, e, i) are often visible in affected NPC and TD cells (scale bars: a: 10 µm, f: 2 µm, h, i: 1 µm, b, c, d, e, g, insets on panel a: 500 nm, inset on panel f: 200 nm).

showed a significant decrease in MPS II NPCs ($p < 0.05$), and a tendency to increased expression in all MPS II affected TD35 samples compared to the Ctrl (Fig. 5; Fig. S6). However, RAB7 (Fig. 5l) and RAB2 (Fig. S6) were not significantly different in any cultures. All these data, together with the previously described LAMP2 expression (Fig. 3), collectively indicate the involvement of the late endosomal-lysosomal (RAB7, LAMP2 and CATD positive) compartment in storage and clearance of accumulated material in MPS II.

3.9. Primary storage vesicles are not a part of the endosomal compartment

Extracellular materials destined for degradation, including GAGs, enter the ELS. To trace this pathway, we treated cells with nanogold particles to identify endosomal-lysosomal elements and to evaluate whether there was a connection with Pr storage vesicles. Ctrl and MPSII-2.5 NPCs were incubated with 5 nm TMA-coated gold nanoparticles [33] at different concentrations (0.5 µM and 1 µM) and treatment times (12 and 24 h). Using electron microscopy, we detected nanogold particles on the plasma membrane, and in Glo and Sq type storage vacuoles, but never in Pr vesicles (Fig. S8). These observations support the hypothesis that the content of Pr vesicles does not originate from the ECM.

3.10. Rough endoplasmic reticulum (RER) and Golgi deformations are characteristic of MPS II affected iPSC derived neuronal cells

Alteration of RER morphology was observed in all MPS II affected NPC and TD35 cultures. Dilated cisterns were frequently documented in

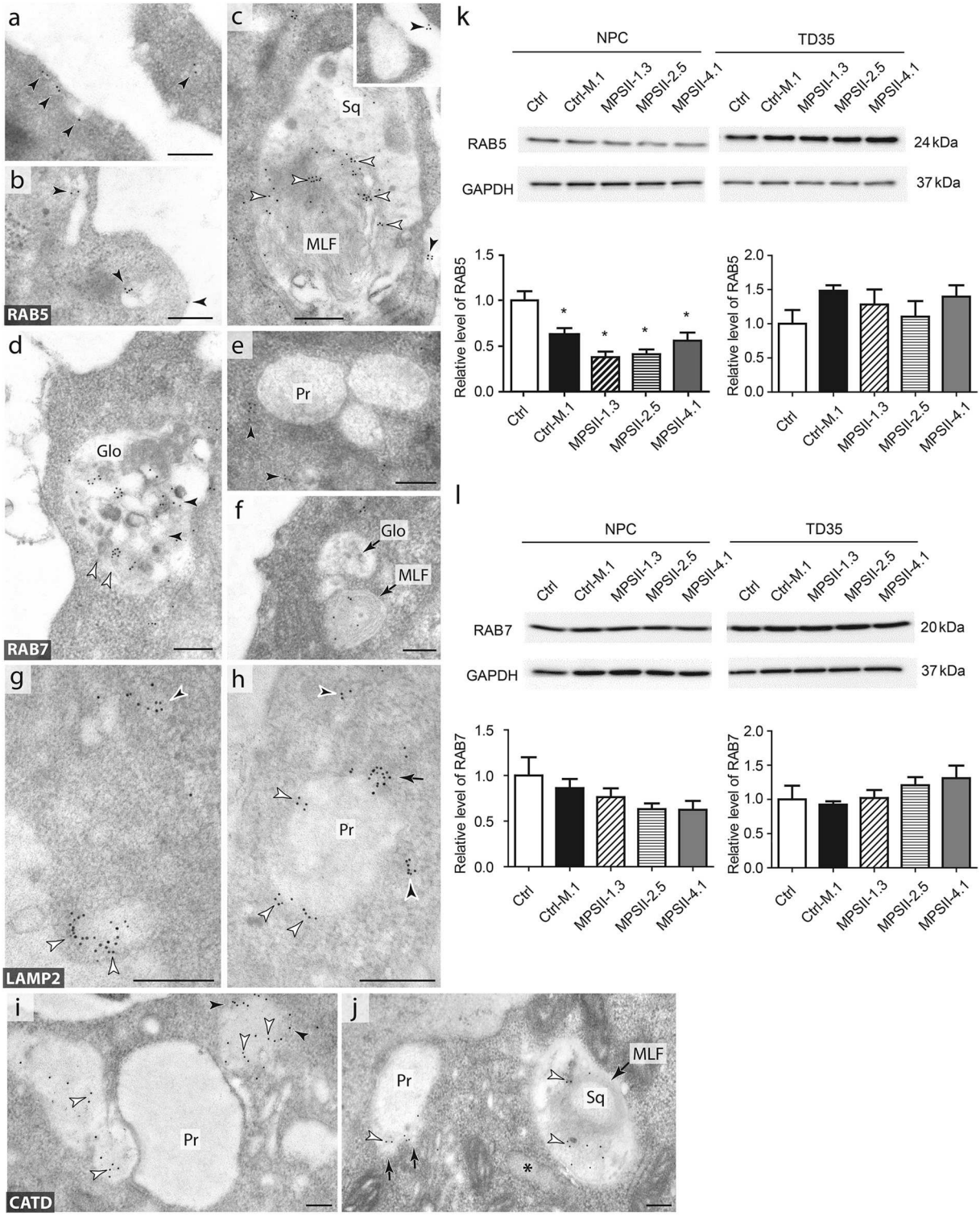

Fig. 5. RAB5, RAB7, Cathepsin D and LAMP2 expression in MPS II disease neuronal cells. **a-j**) immunogold labelling in NPC cultures. **a-c**) RAB5 immunopositivity can be detected on cell surface (black arrowheads in panel b, c and inset in panel c), in internalizing pits (a) and in early endosomal elements near to the plasma membrane (b). A sequestered (Sq) storage vacuole contains multilamellar membrane structure (ML) in panel c. RAB5 specific gold particles can only be detected on internalized membrane whirl (white arrowheads). Inset demonstrates an immuno-negative primary storage vesicle. **d-f**) Immunogold particles decorate some globular type storage vacuoles (d) and multilamellar figure (MLF in panel f) after RAB7 immunolabelling. Immuno-negative primary (Pr, panel e) and globular (Glo, panel f) vesicles can be seen as well. Black arrowheads on panel e indicate small RAB7 positive cytoplasmic vesicles. **g-h**) LAMP2 immunopositive vesicles in the cytoplasm. g) Arrangement of gold particles on smaller (black arrowheads) and larger vesicles (white arrowheads). h) Primary storage vesicle with LAMP2 immunopositive limiting membrane (white arrowheads). Small cytoplasmic vesicles (black arrowheads) seem to be fused with the limiting membrane (black arrow; scale bars: 200 nm). **i-j**) Cathepsin D (CATD) immunopositivity is observable at the limiting membrane (black arrowheads on panel i) and at the inner content (white arrowheads on panel j) of storage vacuoles (MLF – myelin figure, Sq – sequestered type vacuole). Primary vesicles (Pr) are immuno-negative and able to fuse with immunopositive small vesicles (black arrows on panel j). **k-l**) Western blot analysis confirmed the protein expression of RAB5 (k), RAB7 (l) in NPC and TD35 cell lysates. Signals were normalized to GAPDH, data are presented as mean ± SEM (n = 3). Dunnett's test was performed to evaluate the significance of groups compared with the control (Ctrl). *$p < 0.05$).

NPCs, even in the carrier Ctrl-M.1 cells (Fig. 4b and c). Wide ribosome decorated cisterns (Fig. 4d and e) were the most striking in the MPSII-1.3 cells, whereas ribosome-free swollen cisterns with globular endings were found in MPSII-4.1 NPCs (Fig. S4c). There were fewer dilated RER cisterns in MPS II TD35 neuronal cells than in NPCs, although swollen morphology was detected in astrocytes (Fig. S4) and neurons (Fig. S4) as well in all MPS II TD35 cultures.

Storage vesicles often clustered in Golgi areas in both MPS II NPC (Fig. 4e; Figs. S4b–c) and TD35 (Fig. 4g; Fig. S4g) cells. Golgi complexes showed characteristic deformations in all the disease affected cell lines:

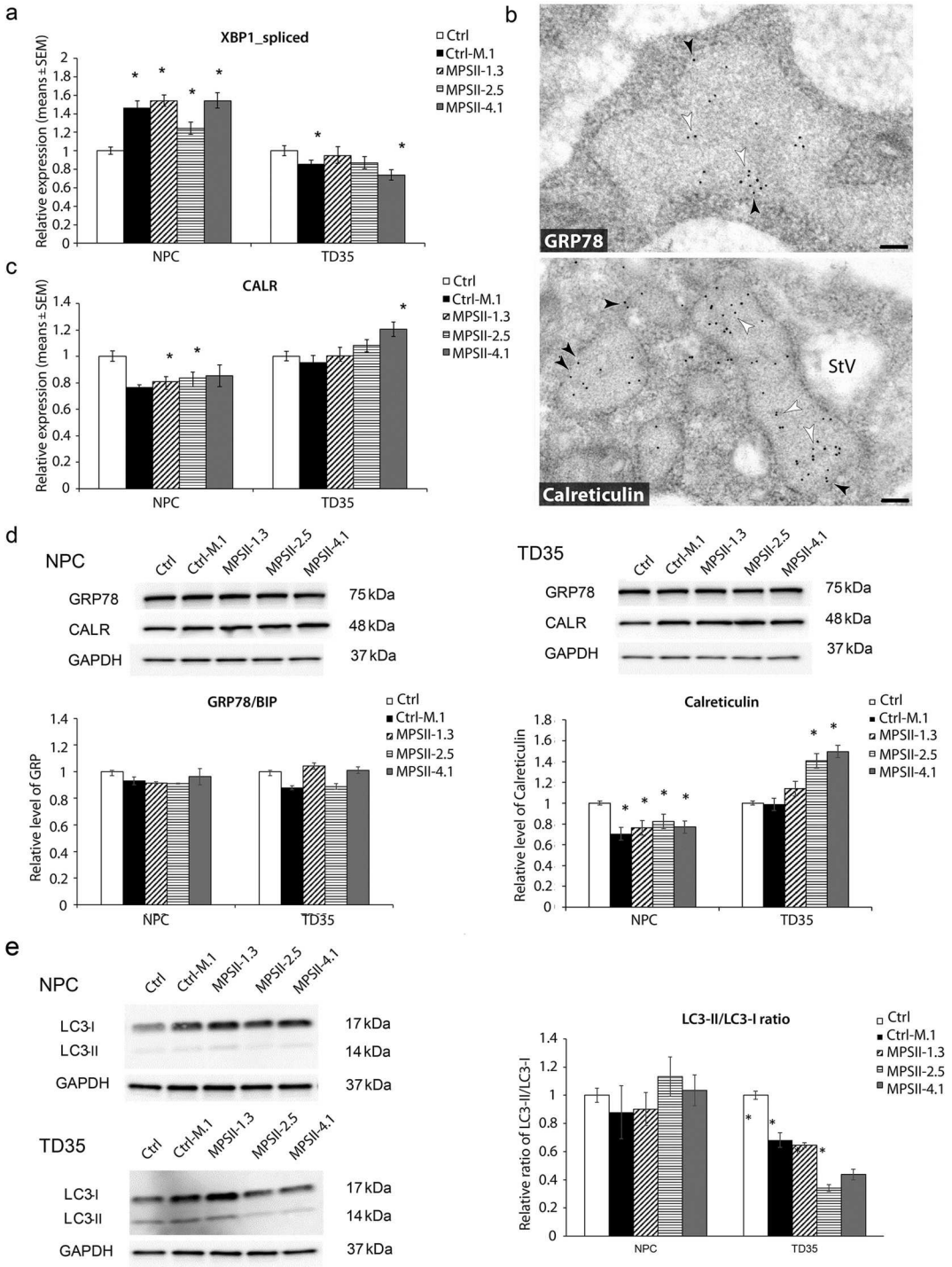

Fig. 6. Endoplasmic reticulum stress and autophagy in MPS II neuronal cultures. a) RT-qPCR assay of XBP1(S) of iPSC derived NPCs and TD35 samples. Values are expressed as relative expression normalized to the NPC control; **b**) Representative RER cisterns after localisation of ER chaperones in MPSII-1.3 NPCs. Although some gold particles associate to ER membrane (black arrowheads), the larger amount of GRP78/BIP and Calreticulin proteins can be visualized in the lumen of dilated RER cisterns (white arrowheads) (StV – globular storage vacuole; scale bars: 100 nm); **c**) Expression of CALR gene in patients' and control NPC and TD35 cultures evaluated by RT-qPCR. Values are expressed as relative expression normalized to the Ctrl, set as 1. Data are presented as mean ± SEM (n = 3). *p < 0.05; **d**) Western-blot analysis of GRP78, Calreticulin, **e**) LC3-I and LC3-II proteins in NPC and TD35 samples. LC3-II/LC3-I ratio was determined and presented. Signals were normalized to GAPDH, Ctrl was set as 1, data are presented as mean ± SEM (n = 3). Dunnett's test was performed to evaluate the significance of groups compared with control (*p < 0.05).

fragmented cisterns, skein-like motifs, onion-like stacks, vacuolation and individual Golgi stacks were frequently documented (Figs. S9b–d). Ribbon and cistern fragmentation were atypical and vacuolation was not observed in healthy Ctrl samples (Fig. S9a).

In summary, ultrastructural examination revealed RER and Golgi deformations in all iPSC derived MPS II and carrier Ctrl-M.1 NPCs and TD35 cells. Based on these observations we can assume the existence of ER and Golgi stress in both NPCs and TD35 neuronal cells. According to our knowledge our study is the first one that documents morphological characteristics of both ER and Golgi stresses in human neuronal cells derived from MPS II patients.

3.11. ER-stress is involved in MPS II associated neurodegeneration

Next, we investigated whether the directed neural differentiation toward NPCs is concomitant with endoplasmic reticulum (ER) stress in patient and control cell lines using the XBP1-assay. This assay relies on the observation that upon accumulation of unfolded proteins in the ER, a 26-nucleotide fragment from the X-box binding protein 1 mRNA ((XBP1(U)) is removed by a special splicing mechanism [38]. This shorter mRNA ((XBP1(S)) is a frequently used marker of ER-stress. First, RT-qPCR assay of the XBP1(S) was performed following the previously described procedure [39]. Interestingly, all MPS II and the carrier NPCs showed upregulation of XBP1(S) compared to the control ($p < 0.05$), whilst TD35 neurons had a different expression pattern (Fig. 6a).

The possibility of stimulated ER stress signalling pathways was studied by immunolabelling ER chaperones on ultrathin sections. Intense accumulation of GRP78/BIP and Ca^{2+} binding ER chaperone calreticulin (CALR) was detected in extremely dilated RER cisterns of each MPS II culture (Fig. 6b), but in relatively few cells. The studied ER chaperones were not detectable in Pr storage vacuoles. There was decreased gene expression of CALR in all MPS II NPCs ($p < 0.05$), with significantly increased expression observed only in MPSII-4.1 TD35 samples ($p < 0.05$; Fig. 6c). Moreover, when cell lysates were investigated with Western-blot CALR expression level was significantly lower ($p < 0.05$) in all MPS II affected NPCs compared to the control. In contrast, the expression of CALR was significantly increased in two of the MPS II TD35 neuronal cultures (Fig. 6d). There were no significant differences in the GRP78/BIP protein expression pattern in all NPC samples (Fig. 6d). In conclusion, the observed disease-specific splicing pattern of XBP1 in NPC stage and elevated calreticulin expression level in two of the TD samples, indicating the involvement of ER-stress in the MPS II cytopathology.

3.12. Autophagy activation

The activation of autophagosome markers was then investigated, to test whether accumulated storage vacuoles and deformed Golgi stacks could induce autophagy as an effective clearance mechanism to eliminate unwanted and damaged cell organelles. Western-blot revealed constant, low levels of both LC3-I and LC3-II in NPCs, with no significant differences between the cell lines ($p > 0.05$) (Fig. 6e). In contrast, in TD35 neuronal cultures Ctrl-M.1 and MPS II patient samples showed significantly higher LC3-I expression than the Ctrl. However, LC3-II form level was significantly higher in the carrier cell line and the MPSII-1.3 patient's sample, while it was the same as of the Ctrl in the MPSII-2.5 and the MPSII-4.1 TD35 cultures (Fig. 6e). We found that LC3-I/LC3-II ratio was significantly lower in MPS II affected TD35 cell cultures than in Ctrl (Fig. 6e). Taken together, these data indicate that the autophagy was affected by the examined IDS mutations of MPS II disease.

4. Discussion

By definition, individual rare diseases affect only a minority of the population but taken together they have a prevalence of > 6% of the world population. Due to the small number of specific patients and their wide phenotypic heterogeneity, very few studies have elucidated the pathophysiological mechanisms of individual rare diseases, so there is still a lack of available treatment for > 60% of them. The group of lysosomal storage disorders (LSDs) is one set of rare diseases where the intensification of pathophysiological studies would be important. Pluripotent stem cell-based research such as disease modelling, drug screening, and possible clinical translation involving gene therapy are potential applications in the LSD disease family.

Currently 11 LSDs have been modelled by human iPSCs, highlighting the importance of the field and the potential of the technology (reviewed in Ref. [46]). To explore novel therapeutic pathways and to address an unmet medical need, we established and described a novel iPSC-based cellular model which recapitulates the MPS II phenotype *in vitro* while identifying an unknown neurological pathomechanism. The disease-specific iPSC lines were capable of NPC production following directed differentiation toward the neural lineage, but their remarkably impaired self-renewal/proliferation capacity revealed the MPS II phenotype at the early progenitor stage. However, terminal differentiation of the NPC cultures revealed mature neuronal cultures, which were demonstrated on protein expression level and detecting synaptic connections with electron microscopy as well. Detailed ultrastructural analysis in concert with transcriptomic and proteomic investigations of the NPC and terminally differentiated stages have led us to the following findings: i) the disease specific storage vacuoles accumulate in patient-derived NPCs and terminally differentiated neuronal cultures and are already present in primary PBMCs; ii) primary storage vesicles seem to be the most prevalent in the disease, although other vacuoles can be clearly identified in the diseased neuronal cell types; iii) the degradation of accumulating material is noticeably impaired; iv) calreticulin upregulation, dilated ER cisterns and Golgi malformations are part of a cytopathology in the TD state; and finally v) in addition to NPCs, both astrocytes and neurons are affected.

4.1. iPSC based MPS II disease model recapitulate IDS deficiency, GAG and storage vacuole accumulation

The discovery of human iPSCs [47,48] opened opportunities to study disease progression during development and to investigate the disease affected cell types in humans via disease specific iPSC differentiation. Tolar et al. generated Hurler syndrome (MPS IH) specific-hiPSCs and demonstrated the potential of gene corrected autologous hematopoietic stem cell production [49]. In MPS II there is only one report on hiPSC generation, where the cells were derived from a symptomatic MPS II female patient where skewed X-chromosome inactivation caused the expression of the mutant IDS allele [50]. Although the results are important regarding the diversity of the disease, neither the cytopathology nor the mechanism of neurodegeneration was investigated. We generated MPS II carrier and diseased human iPSC lines [23,25,26], along with a healthy control, and used these lines as a model system in this study to investigate MPS II cytopathology, focusing on the as yet poorly understood neurodegenerative involvement. Intracellular accumulation of lysosomal storage vacuoles is a cytopathologic hallmark of most LSDs. The ultrastructural morphology of vacuoles is revealed in some LSDs and some cell types, and the correlation between GAG accumulation and presence of storage vesicles in MPSs is long-established [41]. Although the cytopathology of neurodegeneration in MPS II disease is unknown and details are still not clear, the connection between perturbed IDS enzyme activity and GAG turnover and dysfunction of the ELS, ER, Golgi and mitochondria has been documented in various LSDs [41]. When we studied IDS enzyme activity and GAG accumulation, we found decreased IDS enzyme activity and increased GAG accumulation in patient iPSCs and their neuronal derivatives. Moreover, increased storage vacuole accumulation was detected in the diseased cells, similar to that in the patients' original PBMCs. Together these data demonstrated that our iPSC based

in vitro cellular system could adequately model MPS II cytopathology and so could be used for the further study of MPS II.

4.2. Disease phenotype is already apparent in the NPC stage

Our results showed that the NPC stage neuronal differentiation capacity is seriously affected in MPS II disease. NPCs are dividing precursor cells with an active metabolism that is required to form highly complex neural structures. ECM is important for proper cell growth, thus disturbance in GAG metabolism can interrupt proliferation and could influence differentiation [51]. This was clearly demonstrated by the decreased proliferative capacity of late passage MPS II NPCs and by the loss of PAX6 expression. This was in line with morphological changes, such as when the non-dividing cells became post-mitotic and started to grow neurites. As ECM components, heparan sulphate proteoglycans (HSPG) bind numerous ligands such as fibroblast growth factors (FGFs) which are essential for NPC proliferation and regeneration both *in vivo* and *in vitro* [21,52,53]. Upon IDS enzyme dysfunction HSPG metabolism is disturbed, possibly impairing the binding of bFGFs and affecting the self-renewal/proliferative capacity which leads to differentiation.

Additional pathological hallmarks of MPS II observed in NPC cultures were elevated levels of primary storage vesicles in those of MPS II patients, as detected by electron microscopy and by protein expression of lysosome-associated membrane glycoprotein 2 (LAMP2). However, we did not detect GAG accumulation at the NPC stage, finding decreased intracellular GAG levels compared to the controls. In parallel, we also documented a significantly lower level of RAB5, and the same level of RAB7, as in healthy or carrier control NPCs. RAB5 has a central role in clathrin-mediated endocytosis, early endosome formation and maturation [54]. While RAB5 is associated with the pathway that performs uptake of membrane surface receptors and extracellular material, RAB7 manages both the endosomal and autophagosomal pathways, thus the size of the RAB7+ compartment is also related to the level of macroautophagy (MA) [55]. The RAB7+ vesicles transport their material to the RAB7 and LAMP2 double positive lysosomal compartment in healthy cells (Fig. 7a).

A lower rate of endocytosis has been documented in fibroblasts from patients with several types of LSDs (type A Niemann-Pick, type C Niemann-Pick, Fabry and Gaucher diseases) [56], MPS II and MPS IV diseases [57]. These data are consistent with the significantly lower level of RAB5 detected in iPSC derived MPS II NPC cultures, which could limit the rate of endocytosis in these cells.

Both endocytic and autophagic pathways deliver materials into the lysosomal RAB7+ and LAMP2+ compartment (see Fig. 7a). MPS II NPC cell lines showed no LC3-I upregulation, therefore we can assume that this pathway does not load this compartment significantly. Proliferation and cell death provide a good possibility to manage accumulation of intracellular GAGs and damaged cell organelles at tissue level, therefore it may be an adaptive response to LSD, even if it leads to premature differentiation.

We hypothesize that the intensity of GAG uptake decreases due to a reduction of accessible RAB5 (RAB5+ membranes were enclosed in storage vacuoles), and because NPCs are able to exocytose intracellular GAGs. It is known that both late endosomes (multivesicular bodies) and lysosomes can fuse with the plasma membrane to release their contents to the extracellular space (Fig. 7a), even if they stored undigested material. Although this unconventional mode of secretion is poorly understood, induction of this pathway via the overexpression of transcription factor EB (TFEB) reduced the storage material load and LAMP1 compartment in a muscle cell culture system and a mouse model of Pompe disease [58], in mouse models of MPS IIIA (Sanfilippo syndrome), and in a multiple sulfatase deficiency (MSD) model [59], which was in accordance with our TFEB immunolocalization data. In addition to TFEB, mammalian RAB2 has also been found to promote late endosomal exocytosis in cancer cells [60]. In accordance with these

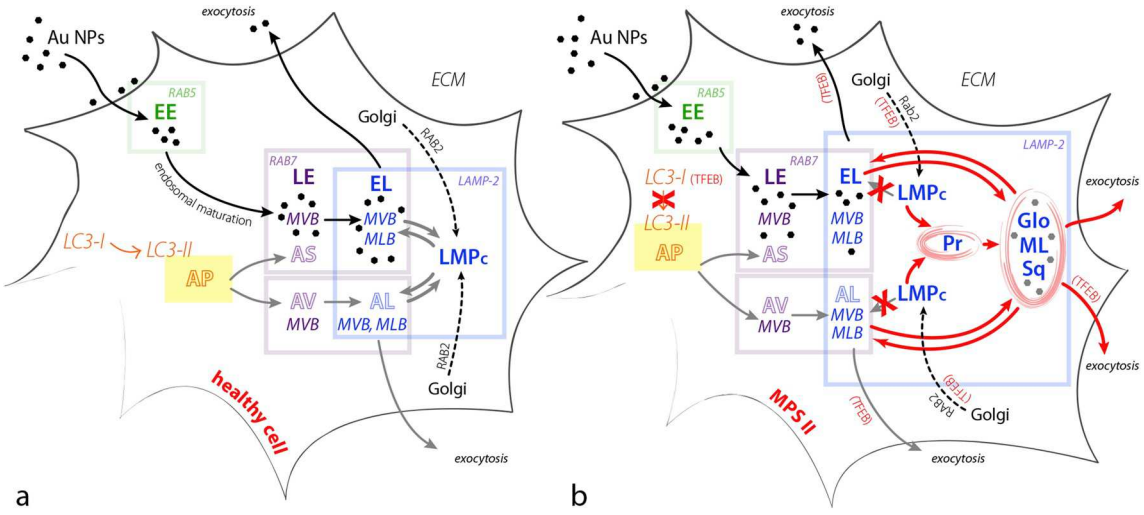

Fig. 7. Model of endocytic and autophagic pathways of healthy and MPS II disease astrocytes. a) Pathways and detected vesicles in healthy cells. Gold nanoparticles (Au NPs) taken up from extracellular matrix (ECM) are transported through the endocytic pathway. Gold particles enter the cell and get into the RAB5+ early endosome (EE) then reach the RAB7+ late endosomal compartment (LE) due to endosomal maturation. Golgi derived RAB2+ lysosomal membrane protein carrier (LMPc) vesicle carries LAMP2 and other lysosomal membrane components and forms endolysosome (EL) by fusing with the LE element. A part of the lysosomal membrane with integrated proteins is able to pinch off from functioning endolysosome for recycling (see grey arrows between LMPc and EL). Undigested materials like gold particles may leave the cell via lysosomal exocytosis. Autophagosome formed by the contribution of LC3-I conversion to LC3-II changes to RAB7+ autophagic vacuole (AV) by maturation or fuses with late endosomal element to form amphisome (AS). Fusion of autophagic vacuole and LMPc results in a RAB7+/LAMP2+ autolysosome (AL). Multivesicular bodies (MVB) and multilamellar bodies (MLB) may be a part of both RAB7+ and RAB7+/LAMP2+ compartments and may contain material of extra- and intracellular origin as well. **b)** Pathways and vesicles in MPS II disease cell. Note that LMPc vesicles do not fuse with RAB7+ late endosomal elements (LE) or autophagic vacuoles (AV), but unite to form a primary storage vesicle (Pr). Gold particles label the early (EE) and late (LE, EL) endosomal elements but do not reach primary vesicles. Primary vesicles are able to fuse with nonfunctional LAMP2+ lysosomes to form globular (Glo), multilamellar (ML) and sequestered (Sq) type storage vacuoles, which contain gold particles. Undigested material accumulates by shuttling between functional RAB7+/LAMP2+ endolysosome (EL) and nonfunctional LAMP2+ compartment. TFEB promotes RAB2+ LMPc production by Golgi, lysosomal exocytosis and LC3-I transcription as well, although LC3 maturation is probably inhibited in MPS II disease.

data, our ultrastructural investigation revealed the presence of RAB7, CATD and LAMP2 positive storage vacuoles from the very moment of exocytosis taking place in NPC cultures. This mechanism can explain how cerebrospinal fluid in the CNS could concentrate GAGs and GAG fragments. To our knowledge this is the first study which has explored the developmental aspects of the disease in neuronal tissue.

4.3. Involvement of ELS by impaired GAG degradation in mature neurons and astrocytes

In contrast to NPCs, mature neurons and astrocytes (TD35) of the two patient cell lines with PTC showed significantly increased intracellular GAG accumulation, while the RAB5, RAB7, and LAMP2 levels were similar to those in a healthy Ctrl sample. Accordingly, we can hypothesize that neither the endosomal nor lysosomal compartment was responsible for GAG accumulation in the siblings' cell lines. However, the patient cell line with the missense mutation did not differ significantly from the control in any of these parameters, consequently MPSII-4.1 TD35 cells did not accumulate GAGs. These conclusions raise the possibility of disturbances of the autophagy pathway, and alteration of neuronal differentiation.

4.4. Autophagosome formation is induced in neuronal cultures of MPS II cell lines

In our experiments, a significantly increased level of LC3-I was detected in all MPS II affected TD35 cultures, consistent with the thought that increased basal autophagy is part of the cytopathology of most LSDs [61]. The role of the mammalian target of rapamycin (mTORC1) in MA regulation is widely discussed. Impaired lysosomal functions attenuate mTOR activity, leading to the activation of TFEB signalling and resulting in the activation of both lysosomal [62,63], and autophagy genes [63]. A predominant nuclear localisation of TFEB has been detected in cultured cells [64] and in a mouse model [62,65] of MPS II. In our study, we observed similar localisation of TFEB protein, with clear dominance in the nuclei of diseased cells of MPS II patients (Fig. 3e). Documented mitochondrial dysfunction in LSDs [66] necessarily increases the cytoplasmic AMP/ATP ratio [67], which can also influence mTOR activity through an AMP-activated protein kinase (AMPK) pathway [68,69].

Involvement of autophagy in the self-renewal and differentiation of neural progenitor cells is well known [70]. Based on the increased LC3-I level, we hypothesize that both AMPK and TFEB pathways might be activated in MPS II neurons and astrocytes, where autophagosome formation was induced.

4.5. MPS II impair LC3 processing in TD35 cultures

We detected a significantly lower LC3-II/LC3-I ratio in all MPS II affected cultures in contrast to the Ctrl sample. Macroautophagy is a highly organized degradation pathway essential for cellular homeostasis, survival and differentiation. Initiation of MA is a multistep process that involves the formation of an isolating membrane (phagophore) that closes to form a double membrane vesicle, an autophagosome. Association of microtubule-associated protein 1 light chain 3 (LC3) and the isolating membrane is an indispensable step in autophagosome formation. LC3 is synthesized as precursor form (proLC3), which is cleaved to its soluble form LC3-I. Lipidation of LC3-I results in the production of the functional, membrane-bound form, LC3-II. Autophagosomes then undergo maturation into autolysosomes, in which the inner membrane-bound LC3-II is degraded by lysosomal hydrolases [71,72].

Based on some fundamental studies in the field of autophagy [73,74], we hypothesize that there is a low LC3-I→LC3-II transition rate in all MPS II affected TD35 cell cultures. The possibility of impaired autophagosome formation is corroborated by our only rare observation of autophagosomes in MPS II TD35 cells in ultrastructural studies. Because autophagosome accumulation is thought to be common in many storage diseases [72], our findings could extend the knowledge on the cytopathology of LSDs.

4.6. Identity of storage vacuoles

The size of the RAB7 positive compartment was not affected in MPS II neuronal cells, even though the LAMP2 level was increased in all MPS II disease cell lines. The LAMP2+ (endo- and autolysosomes) and RAB7+ (late endosomes, endo- and autolysosomes) compartments are partly overlapping in healthy cells, except for newly formed lysosomal membrane carriers generated by the Golgi complex (Fig. 7a). An increase in the LAMP2, but not the RAB7 compartment in MPS II diseased cells surely then implicates the involvement of the lysosomal system in the cytopathology of MPS II.

Theoretically, there are two possible explanations for these results. On the one hand, the increase in the LAMP2 compartment could originate from the loss of the RAB7 marker from the LAMP2 and RAB7 double positive compartment, leading to the accumulation of unidentified storage vacuole material in this compartment. According to the traditional concept, this material would be undigested GAGs that accumulated due to the IDS deficiency. To our knowledge RAB7 is not necessary for lysosomal exocytosis [75], and we proved that the LAMP2 positive compartment is able to clear its storage material via exocytosis. This assumption is compatible with the results of Spampanato et al. who identified that the exocytosed vesicles were both LAMP1 and LC3 positive in Pompe disease [58].

On the other hand, LAMP2 but not RAB7 positive membranes are found on the LAMP-containing biosynthetic carriers released from the Golgi. Lysosomal membrane proteins, like LAMPs, are transported directly to the late endosomal compartment by non-clathrin coated vesicles called lysosomal membrane protein carriers (LMPc) [60]. Golgi derived LMPc are RAB7 negative but may carry Golgi markers (Fig. 7a). In *Drosophila* garland cells RAB2 has been shown to be indispensable for lysosomal membrane protein delivery to late endosomes. Lund et al. reported that LMP carrier vesicles accumulated and seemed to fuse with each other or with non-degradative storage lysosomes in the absence of RAB2 [60]. These results are consistent with our observations that storage vesicles are not necessarily RAB7 or CATD positive but are able to fuse with each other. In addition, we observed small cytoplasmic vesicles that were RAB2 and LAMP2 immunopositive and seemed to fuse with each other.

Since primary storage vesicles are formed by LMP carriers, they are RAB2 and LAMP2 positive and originally contain no GAGs. Vesicles are able to fuse with each other and with RAB7 positive endo- and autolysosomes, meaning that undigested GAGs and inner membranes enter storage vesicles indirectly, via endolysosomes. The resulting Glo, ML and Sq types of storage vacuoles may recycle into a LAMP2 positive and RAB7 negative compartment (see Fig. 7a).

Involvement of the Golgi in MPS cytopathology in MPS IIIB (Sanfilippo syndrome) caused by mutation of N-acetyl-alpha-glucosaminidase (NAG) was suggested by Vitry et al. who detected Golgi matrix 130 (GM130, also known as golgin subfamily A member 2, GOLGA2) and LAMP-1, but not early endosome antigen 1 (EEA1) marker on storage vacuoles of cortical neurons in a mouse model. In their comprehensive study they demonstrated that storage vacuoles did not receive materials from the endocytic pathway [76]. These data are consistent with our results related to the early endosomal compartment, i.e. that the limiting membrane of each storage vacuole types was RAB5 negative, and we did not detect functionalized nanoparticles in primary storage vesicles, although gold particles appeared in Glo, ML and Sq type vacuoles (Fig. 7b).

However, Vitry et al. found that the autophagic pathway was not affected in MPS IIIB, as the same LC3 pattern was detected by Western blot in both diseased and control cortical cultures [76]. While this latter

observation is the same as ours in iPSC derived NPC cultures, MPS II TD35 cells showed higher LC3-I level than Ctrl cell lines. Finally, Vitry et al. observed Golgi deformations including wider cisterns, internal bulbs and dilated saccules in MPS IIIB cortical neurons and suggested the impact of Golgi complex disorganisation in the formation of the cytopathology [76]. We detected very similar deformations in Golgi structure in the iPSC derived MPS II model. To determine whether Golgi stress has a role in initiating the formation of storage vacuoles, or it is an outcome of disturbances in the lysosomal and/or ER compartment needs detailed examination.

4.7. Role of ER in MPS II cytopathology

Our first observation related to ER stress was the frequent occurrence of dilated ER cisterns both in MPS II NPC cells and TD35 cultures. In response to stress conditions, like accumulation of misfolded proteins or Ca^{2+} depletion in ER cisterns, GRP78/BIP dissociates from UPR (unfolded protein response) sensors and translocates from the ER membrane to the lumen, ultimately leading to the alternative splicing of transcription factor XBP1 (X-box binding protein 1) mRNA (XBP1(U)). The shorter XBP1 mRNA (XBP1(S)) is frequently used as a marker of ER stress, but while we found a significantly increased level of XBP1(S) in MPS II NPCs, this seemed to be independent of the levels of two examined ER chaperones, GRP78/BIP and calreticulin.

Involvement of the UPR in LSDs is controversial. The possibility of UPR activation in LSD pathogenesis may be influenced by tissue type, extent and type of the accumulated substance, and the type of the mutation. Although Villani et al. detected no XBP1(S) in human MPS II fibroblast cells [77], we have demonstrated significantly elevated level of the spliced form of the XBP1 in MPS II neuronal progenitor cells. Accordingly, we can state that ER stress is involved in the cytopathology of MPS II in neuronal cells in NPC stage, and it presumably activates the IRE1 (inositol-requiring kinase 1) signalling pathway. Although ER stress is able to induce apoptosis [78], the IRE1 pathway is thought to be an adaptive, anti-apoptotic branch of UPR [79], which explains why we did not find elevated caspase 3/7 activity in patient derived NPCs.

In contrast to the NPC state, the IRE1 branch of UPR was not active (see the XBP1(S) levels) and GRP78/BIP and calreticulin seemed to be slightly upregulated in TD35 cultures. Calreticulin is the primary calcium-buffering chaperone of the RER, implicated in both the storage and release of Ca^{2+} from ER cisterns [80,81]. We assume that Ca^{2+} depletion from the ER caused the increased cytoplasmic Ca^{2+} level in MPS II TD35 cells. The elevation of cytoplasmic Ca^{2+} is thought to be a significant problem in LSD affected cells due to the impaired sequestering capacity of damaged mitochondria [66]. Sustained elevation of cytoplasmic Ca^{2+} level and increased ion transfer from ER to mitochondrion are thought to have a pro-apoptotic effect [81,82]. In the first case activated calpain-9 (CAN9) cleaves pro-caspase 3/7 [83], in the latter case cytochrome c (CYC) release from damaged mitochondria results in effector caspase activation through Caspase 9 (CASP9) [82,83]. Although we detected a similar amount of pro-Caspase 9 (the uncleaved form) and the cleaved forms in healthy and MPS II TD cultures, it might not correlate the exact activity of the CASP9. The precise mechanism of CASP9 activation is uncleared. Several experimental data indicate that uncleaved pro-Caspase 9 may be activated by dimer formation [84] on a platform provided by cytochrome c binding apoptosome [84]. Thus, the higher band (47 kDa) detected by Western-blot might origin from both inactive zymogen and the active, unprocessed CASP9 forms. Cleaved CASP9 thought to be involved in timing function in apoptosis induction [85]. Although we measured CASP3/7 activity, we assume that the significantly high CASP3/7 activity in all disease-affected TD cultures refers to elevated CASP9 activity. Although the ratio of uncleaved and proteolytically cleaved CASP9 is not affected by MPS II disease, knowing the complex regulation of CASP9 activity [84] we suppose that this balance is shifted towards the inhibition of cell death in healthy cells and towards the initiation of apoptosis in MPS II cells.

Taken together, our findings suggest the depletion of luminal Ca^{2+} storage of ER, elevated ion concentration in cytoplasm and increased sensitivity to apoptosis in MPS II neuronal and glial cells. We found significantly higher Caspase3/7 activity in patient derived TD35 cultures compared to the healthy Ctrl and carrier Ctrl-M.1 samples which might be related to both apoptosis and synaptic pruning in the maturing neuronal cultures.

4.8. Astrocytes are the primarily affected cells in MPS II neuronal cultures

In one of the LSDs, multiple sulfatase deficiency (MSD), caused by mutations in the sulfatase modifying factor 1 (*SUMF1*) gene [86], massive vacuolisation of GFAP positive astrocytes in the brain of *sumf1* mutant mice has been reported. Vacuoles co-localized with ubiquitin positive aggregates in both neurons and microglial cells corresponding to the cytoplasmic increase of P62/SQSTM1 [86]. In our study we observed increased LAMP2+ vacuolisation in GFAP positive astrocytes in the patients' TD35 samples. Interestingly, this phenotype was observed in some of the carrier mother (Ctrl-M.1) neuronal samples as well, suggesting she was affected by the disease at the cellular level. MPS II neuronal cultures showed massive storage vacuole accumulation with increased cell death (increased Caspase 3/7 activity and LC3 level), which was more prevalent in astrocytes. This cell type specific difference might be in correlation with the role of astrocytes in the CNS, as they supply energy to neurons, maintain brain homeostasis through multiple dynamic equilibrium adjustments and recycling, and protect neurons against oxidative stress [87]. Astrocyte dysfunction is observed in numerous LSDs and is suggested to impact neurodegeneration [88], as in several other neurodegenerative disorders [87]. Our results demonstrate that when astrocytes are impaired in their ability to support differentiation and survival of cortical neurons, it may lead to cell death and neurodegeneration at the tissue level.

4.9. Are carriers asymptomatic on a cellular level?

We have to draw attention to the parameters of the carrier Ctrl-M.1 cell line. MPS II is an X-linked, recessive disorder: female carriers are healthy with a mutant and a wild-type allele. We identified storage vacuoles as cytopathological hallmarks of MPS II in her iPSC derived NPCs and TD cells, albeit rarely, despite her apparently healthy phenotype.

X chromosome inactivation (XCI) is transcriptional silencing of maternal or paternal X chromosome in female mammals. XCI patterns vary from tissue to tissue [89], therefore females are mosaic for the expression of X-linked genes [90]. Although symptomatic female carriers were documented in cases of Fabry [91] and Hunter disease [92], the XCI pattern was not correlated with enzymatic levels of α-Galactosidase A or IDS enzyme, respectively [91]. We know that XCI is incomplete in humans, and the identification of the IDS gene as "inactive" and not an "escape" gene was made in a comprehensive study by Tukiainen et al. [93]. However, upon genetic reprogramming the epigenetic pattern of founder cells changes, which could lead to altered expression following tissue specific differentiation of the reprogrammed cells [94,95].

5. Conclusion

To our knowledge, our study is the first comprehensive characterisation of MPS II affected neuronal cells *in vitro*. We documented an elevated level of lysosomal marker LAMP2 and a decreased level of intracellular GAG accumulation in our iPSC derived NPC and neuron cultures and provided two possible explanations for the origin of storage vacuoles. One of them is based on the traditional concept that focuses on an endocytic origin of storage vesicles and considers them to be part of the disturbed lysosomal system. The other hypothesis highlights the possible central role of LMP vesicles in the formation of storage vacuoles, but indicates further questions, regarding UPR induction or the reason behind the impaired fusion between LMP carriers

and functional lysosomes in MPS II.

We established and defined an iPSC based *in vitro* cellular model for the study of MPS II cellular pathology. We concluded that NPC cultures could provide a good model system for the examination of basic cytopathological events in MPS II, because NPC cultures showed more similarity with disease-associated parameters than TD35 cultures despite their genetic background. In contrast, TD35 cultures provide an effective *in vitro* model for the study of the involvement of different cell types in the cytopathological features of the disease. Although our system was used for modelling disease neuropathology, the pluripotent nature of iPSCs means that it offers a tool for drug testing, gene therapy studies, and further study to understand the disorder at the cellular level, in a range of cell types that are seriously affected by this disease, which currently has no efficient treatment. Our study provides novel information on the advancement of the disease, which opens the possibility of finding biomarkers helping to identify the disease as early as possible.

Ethics approval and consent to participate

Written informed consent had been obtained from the subjects who provided their samples for iPSC derivation. Ethical approvals were obtained from the Medical Research Council (in Hungarian: Egészségügyi Tudományos Tanács; ETT) to establish and maintain hiPSC lines (ETT-TUKEB 834/PI/09, 8-333/2009-1018EKU).

Consent for publication

Not applicable.

Availability of data and material

Additional files are made available online along with the manuscript.

Conflicts of interest

The authors declare that they have no competing interests.

Funding

This work was supported by grants from European Union's FP7-PEOPLE programme (Anistem, PIAPP-GA-2011-286264; STEMMAD, PIAPP-GA-2012-324451; EpiHealthNet, PITN-GA-2012-317146). Maria Lo Giudice has received funding from 'The CaSR Biomedicine Network' from the Marie Sklodowska-Curie Actions of the European Union's Horizon 2020 programme under REA grant agreement no. 675228.

Authors' contributions

JK designed the study, was involved in the implementation of the experiments, data analysis, and wrote the manuscript. **KM** and **BJ** performed the electron microscopy analysis, participated in the interpretation of the results, wrote and reviewed the manuscript. **EV** established and characterized the iPSCs, implemented part of the cell culture experiments, analysed the data and participated in the interpretation of the results. **IB** performed, analysed and interpreted the molecular biology experiments; **SZ** was involved in neural induction of iPSC lines; **AT** did cell culture work and performed GAG measurements; **MLG** performed Western-blot experiments; **MHW** and **WWMPP** performed I2S enzyme assay; **PP** was involved in immunocytochemistry and fluorescent microscopy; **NV** provided clinical data of the patients; **LL** analysed electron microscopy data, and participated in the interpretation of the data; **HN** provided the nanogold particles; **NK, KF** and **PH** supervised the experiments; **AD** approved the study design, read and approved the manuscript. All authors read and approved the final version of the manuscript.

Acknowledgements

We would like to thank the Department of Paediatrics, University of Phayao and Dr. Zoltán Nyúl for collecting the patient blood samples and providing clinical data. We are grateful for the help of: Mónika Truszka (Department of Anatomy, Cell and Developmental Biology, Eötvös Loránd University, Budapest H-1117; Hungary), in the preparation of samples for electron microscopy; Dr. Peter Lőrincz (Department of Anatomy, Cell and Developmental Biology, Eötvös Loránd University, Budapest H-1117; Hungary) for methodical advice in electron microscopy; Csilla Nemes (BioTalentum Ltd.) in study design; Eszter Kovács (BioTalentum Ltd.) in cell culture work; Satoshi Teraji (Department of Macromolecular Science and Engineering, Graduate School of Science and Technology, Kyoto Institute of Technology, Matsugasaki, Kyoto 606–8585, Japan) in the preparation of nanoparticles; and István Lagzi (Budapest University of Technology and Economics Department of Physics, H-1111 Budapest) and Róbert Horváth (Nanobiosensorics Laboratory, Centre for Energy Research, Institute of Technical Physics and Materials Science, H-1525 Budapest, Hungary) for their help in nanomaterial uptake experimental design.

Appendix A. Supplementary data

Supplementary data to this article can be found online at https://doi.org/10.1016/j.yexcr.2019.04.021.

References

[1] J. Muenzer, Overview of the mucopolysaccharidoses, Rheumatology 50 (Suppl 5) (2011) v4–12.
[2] P.J. Meikle, J.J. Hopwood, A.E. Clague, W.F. Carey, Prevalence of lysosomal storage disorders, Jama 281 (3) (1999) 249–254.
[3] M. Scarpa, Z. Almassy, M. Beck, O. Bodamer, I.A. Bruce, L. De Meirleir, N. Guffon, E. Guillen-Navarro, P. Hensman, S. Jones, et al., Mucopolysaccharidosis type II: European recommendations for the diagnosis and multidisciplinary management of a rare disease, Orphanet J. Rare Dis. 6 (2011) 72.
[4] E.F. Neufeld, I. Liebaers, C.J. Epstein, S. Yatziv, A. Milunsky, B.R. Migeon, The Hunter syndrome in females: is there an autosomal recessive form of iduronate sulfatase deficiency? Am. J. Hum. Genet. 29 (5) (1977) 455–461.
[5] L.L. Pinto, T.A. Vieira, R. Giugliani, I.V. Schwartz, Expression of the disease on female carriers of X-linked lysosomal disorders: a brief review, Orphanet J. Rare Dis. 5 (2010) 14.
[6] J.E. Wraith, M. Scarpa, M. Beck, O.A. Bodamer, L. De Meirleir, N. Guffon, A. Meldgaard Lund, G. Malm, A.T. Van der Ploeg, J. Zeman, Mucopolysaccharidosis type II (Hunter syndrome): a clinical review and recommendations for treatment in the era of enzyme replacement therapy, Eur. J. Pediatr. 167 (3) (2008) 267–277.
[7] V. Valayannopoulos, F.A. Wijburg, Therapy for the mucopolysaccharidoses, Rheumatology 50 (Suppl 5) (2011) v49–59.
[8] V.A. McKusick, The classification of heritable disorders of connective tissue, Birth Defects Orig. Artic. Ser. 11 (6) (1975) 1–9.
[9] G.M. Pastores, P. Arn, M. Beck, J.T. Clarke, N. Guffon, P. Kaplan, J. Muenzer, D.Y. Norato, E. Shapiro, J. Thomas, et al., The MPS I registry: design, methodology, and early findings of a global disease registry for monitoring patients with Mucopolysaccharidosis Type I, Mol. Genet. Metabol. 91 (1) (2007) 37–47.
[10] J. Muenzer, M. Beck, C.M. Eng, M.L. Escolar, R. Giugliani, N.H. Guffon, P. Harmatz, W. Kamin, C. Kampmann, S.T. Koseoglu, et al., Multidisciplinary management of Hunter syndrome, Pediatrics 124 (6) (2009) e1228–1239.
[11] A.A.M. Vollebregt, M. Hoogeveen-Westerveld, M.A. Kroos, E. Oussoren, I. Plug, G.J. Ruijter, A.T. van der Ploeg, W. Pijnappel, Genotype-phenotype relationship in mucopolysaccharidosis II: predictive power of IDS variants for the neuronopathic phenotype, Dev. Med. Child Neurol. 59 (10) (2017) 1063–1070.
[12] M.H. de Ru, J.J. Boelens, A.M. Das, S.A. Jones, J.H. van der Lee, N. Mahlaoui, E. Mengel, M. Offringa, A. O'Meara, R. Parini, et al., Enzyme replacement therapy and/or hematopoietic stem cell transplantation at diagnosis in patients with mucopolysaccharidosis type I: results of a European consensus procedure, Orphanet J. Rare Dis. 6 (2011) 55.
[13] A. Tanaka, T. Okuyama, Y. Suzuki, N. Sakai, H. Takakura, T. Sawada, T. Tanaka, T. Otomo, T. Ohashi, M. Ishige-Wada, et al., Long-term efficacy of hematopoietic stem cell transplantation on brain involvement in patients with mucopolysaccharidosis type II: a nationwide survey in Japan, Mol. Genet. Metabol. 107 (3) (2012) 513–520.
[14] N. Gomez-Ospina, S.G. Scharenberg, N. Mostrel, R.O. Bak, S. Mantri, R.M. Quadros, C.B. Gurumurthy, C. Lee, G. Bao, L. Aurelian, et al., Human genome-edited hematopoietic stem cells phenotypically correct Mucopolysaccharidosis type I, bioRxiv

(2018) 408757.
[15] R.J. Holley, S.R. Wood, B.W. Bigger, Delivering hematopoietic stem cell gene therapy treatments for neurological lysosomal diseases, ACS Chem. Neurosci. 10 (1) (2019) 18–20.
[16] B. Hoffmann, G. Schulze-Frenking, S. Al-Sawaf, M. Beck, E. Mayatepek, Hunter disease before and during enzyme replacement therapy, Pediatr. Neurol. 45 (3) (2011) 181–184.
[17] J. Muenzer, O. Bodamer, B. Burton, L. Clarke, G.S. Frenking, R. Giugliani, S. Jones, M.V. Rojas, M. Scarpa, M. Beck, et al., The role of enzyme replacement therapy in severe Hunter syndrome-an expert panel consensus, Eur. J. Pediatr. 171 (1) (2012) 181–188.
[18] D.P. Rastall, A. Amalfitano, Recent advances in gene therapy for lysosomal storage disorders, Appl. Clin. Genet. 8 (2015) 157–169.
[19] C. Vogler, E.H. Birkenmeier, W.S. Sly, B. Levy, C. Pegors, J.W. Kyle, W.G. Beamer, A murine model of mucopolysaccharidosis VII. Gross and microscopic findings in beta-glucuronidase-deficient mice, Am. J. Pathol. 136 (1) (1990) 207–217.
[20] J. Muenzer, J.C. Lamsa, A. Garcia, J. Dacosta, J. Garcia, D.A. Treco, Enzyme replacement therapy in mucopolysaccharidosis type II (Hunter syndrome): a preliminary report, Acta Paediatr. 91 (439) (2002) 98–99.
[21] I. Farhy Tselnicker, M.M. Boisvert, N.J. Allen, The role of neuronal versus astrocyte-derived heparan sulfate proteoglycans in brain development and injury, Biochem. Soc. Trans. 42 (5) (2014) 1263–1269.
[22] E. Fusar Poli, C. Zalfa, F. D'Avanzo, R. Tomanin, L. Carlessi, M. Bossi, L.R. Nodari, E. Binda, P. Marmiroli, M. Scarpa, et al., Murine neural stem cells model Hunter disease in vitro: glial cell-mediated neurodegeneration as a possible mechanism involved, Cell Death Dis. 4 (2013) e906.
[23] E. Varga, C. Nemes, I. Bock, N. Varga, A. Feher, A. Dinnyes, J. Kobolak, Generation of Mucopolysaccharidosis type II (MPS II) human induced pluripotent stem cell (iPSC) line from a 1-year-old male with pathogenic IDS mutation, Stem Cell Res. 17 (3) (2016) 482–484.
[24] E. Varga, C. Nemes, I. Bock, N. Varga, A. Feher, J. Kobolak, A. Dinnyes, Generation of Mucopolysaccharidosis type II (MPS II) human induced pluripotent stem cell (iPSC) line from a 3-year-old male with pathogenic IDS mutation, Stem Cell Res. 17 (3) (2016) 479–481.
[25] E. Varga, C. Nemes, I. Bock, N. Varga, A. Feher, J. Kobolak, A. Dinnyes, Generation of Mucopolysaccharidosis type II (MPS II) human induced pluripotent stem cell (iPSC) line from a 7-year-old male with pathogenic IDS mutation, Stem Cell Res. 17 (3) (2016) 463–465.
[26] E. Varga, C. Nemes, E. Kovacs, I. Bock, N. Varga, A. Feher, A. Dinnyes, J. Kobolak, Generation of human induced pluripotent stem cell (iPSC) line from an unaffected female carrier of Mucopolysaccharidosis type II (MPS II) disorder, Stem Cell Res. 17 (3) (2016) 514–516.
[27] S.M. Chambers, C.A. Fasano, E.P. Papapetrou, M. Tomishima, M. Sadelain, L. Studer, Highly efficient neural conversion of human ES and iPS cells by dual inhibition of SMAD signaling, Nat. Biotechnol. 27 (3) (2009) 275–280.
[28] Y. Shi, P. Kirwan, F.J. Livesey, Directed differentiation of human pluripotent stem cells to cerebral cortex neurons and neural networks, Nat. Protoc. 7 (10) (2012) 1836–1846.
[29] Y.V. Voznyi, J.L. Keulemans, O.P. van Diggelen, A fluorimetric enzyme assay for the diagnosis of MPS II (Hunter disease), J. Inherit. Metab. Dis. 24 (6) (2001) 675–680.
[30] H. Nakanishi, K.J. Bishop, B. Kowalczyk, A. Nitzan, E.A. Weiss, K.V. Tretiakov, M.M. Apodaca, R. Klajn, J.F. Stoddart, B.A. Grzybowski, Photoconductance and inverse photoconductance in films of functionalized metal nanoparticles, Nature 460 (7253) (2009) 371–375.
[31] H. Nakanishi, D.A. Walker, K.J. Bishop, P.J. Wesson, Y. Yan, S. Soh, S. Swaminathan, B.A. Grzybowski, Dynamic internal gradients control and direct electric currents within nanostructured materials, Nat. Nanotechnol. 6 (11) (2011) 740–746.
[32] B. Peter, S. Kurunczi, D. Patko, I. Lagzi, B. Kowalczyk, Z. Racz, B.A. Grzybowski, R. Horvath, Label-free in situ optical monitoring of the adsorption of oppositely charged metal nanoparticles, Langmuir : ACS J. Surf. Colloids 30 (44) (2014) 13478–13482.
[33] B. Peter, I. Lagzi, S. Teraji, H. Nakanishi, L. Cervenak, D. Zambo, A. Deak, K. Molnar, M. Truszka, I. Szekacs, et al., Interaction of positively charged gold nanoparticles with cancer cells monitored by an in situ label-free optical biosensor and transmission electron microscopy, ACS Appl. Mater. Interfaces 10 (32) (2018) 26841–26850.
[34] E. Tóth-Szeles, J. Horváth, G. Holló, R. Szűcs, H. Nakanishi, I. Lagzi, Chemically coded time-programmed self-assembly, Mol. Syst. Des. Eng. 2 (3) (2017) 274–282.
[35] D.L. White, J.E. Mazurkiewicz, R.J. Barrnett, A chemical mechanism for tissue staining by osmium tetroxide-ferrocyanide mixtures, J. Histochem. Cytochem. : Off. J. Histochem. Soc. 27 (7) (1979) 1084–1091.
[36] M.A. Berryman, R.D. Rodewald, An enhanced method for post-embedding immunocytochemical staining which preserves cell membranes, J. Histochem. Cytochem. : Off. J. Histochem. Soc. 38 (2) (1990) 159–170.
[37] M.W. Pfaffl, G.W. Horgan, L. Dempfle, Relative expression software tool (REST©) for group-wise comparison and statistical analysis of relative expression results in real-time PCR, Nucleic Acids Res. 30 (9) (2002) e36-e36.
[38] H. Yoshida, T. Matsui, A. Yamamoto, T. Okada, K. Mori, XBP1 mRNA is induced by ATF6 and spliced by IRE1 in response to ER stress to produce a highly active transcription factor, Cell 107 (7) (2001) 881–891.
[39] A. van Schadewijk, E.F. van't Wout, J. Stolk, P.S. Hiemstra, A quantitative method for detection of spliced X-box binding protein-1 (XBP1) mRNA as a measure of endoplasmic reticulum (ER) stress, Cell Stress Chaperones 17 (2) (2012) 275–279.
[40] R. Minami, Y. Watanabe, T. Kudoh, K. Oyanagi, T. Nakao, Fluorometric measurement of alpha-L-iduronidase activity using 4-methylumbelliferyl-alpha-L-iduronide, Tohoku J. Exp. Med. 130 (4) (1980) 381–384.
[41] F.M. Platt, B. Boland, A.C. van der Spoel, Lysosomal storage disorders: the cellular impact of lysosomal dysfunction, J. Cell Biol. 199 (5) (2012) 723–734.
[42] E.J. Parkinson-Lawrence, T. Shandala, M. Prodoehl, R. Plew, G.N. Borlace, D.A. Brooks, Lysosomal storage disease: revealing lysosomal function and physiology, Physiology 25 (2) (2010) 102–115.
[43] T. Lemonnier, S. Blanchard, D. Toli, E. Roy, S. Bigou, R. Froissart, I. Rouvet, S. Vitry, J.M. Heard, D. Bohl, Modeling neuronal defects associated with a lysosomal disorder using patient-derived induced pluripotent stem cells, Hum. Mol. Genet. 20 (18) (2011) 3653–3666.
[44] W.R. Markesbery, R.O. Robinson, P.V. Falace, M.D. Frye, Mucopolysaccharidoses: ultrastructure of leukocyte inclusions, Ann. Neurol. 8 (3) (1980) 332–336.
[45] B.C. Kieseier, H.H. Goebel, Characterization of T-cell subclasses and NK-cells in lysosomal disorders by immuno-electron microscopy, Neuropathol. Appl. Neurobiol. 20 (6) (1994) 604–608.
[46] D.K. Borger, B. McMahon, T. Roshan Lal, J. Serra-Vinardell, E. Aflaki, E. Sidransky, Induced pluripotent stem cell models of lysosomal storage disorders, Dis. Model. Mech. 10 (6) (2017) 691–704.
[47] K. Takahashi, K. Tanabe, M. Ohnuki, M. Narita, T. Ichisaka, K. Tomoda, S. Yamanaka, Induction of pluripotent stem cells from adult human fibroblasts by defined factors, Cell 131 (5) (2007) 861–872.
[48] K. Takahashi, S. Yamanaka, Induction of pluripotent stem cells from mouse embryonic and adult fibroblast cultures by defined factors, Cell 126 (4) (2006) 663–676.
[49] J. Tolar, I.H. Park, L. Xia, C.J. Lees, B. Peacock, B. Webber, R.T. McElmurry, C.R. Eide, P.J. Orchard, M. Kyba, et al., Hematopoietic differentiation of induced pluripotent stem cells from patients with mucopolysaccharidosis type I (Hurler syndrome), Blood 117 (3) (2011) 839–847.
[50] M. Reboun, J. Rybova, R. Dobrovolny, J. Vcelak, T. Veselkova, G. Storkanova, D. Musalkova, M. Hrebicek, J. Ledvinova, M. Magner, et al., X-chromosome inactivation analysis in different cell types and induced pluripotent stem cells elucidates the disease mechanism in a rare case of mucopolysaccharidosis type II in a female, Folia Biol. 62 (2) (2016) 82–89.
[51] S. Sarrazin, W.C. Lamanna, J.D. Esko, Heparan sulfate proteoglycans, Cold Spring Harbor Perspect. Biol. 3 (7) (2011).
[52] C.D. Stern, Initial patterning of the central nervous system: how many organizers? Nat. Rev. Neurosci. 2 (2) (2001) 92–98.
[53] B. Bilican, M.R. Livesey, G. Haghi, J. Qiu, K. Burr, R. Siller, G.E. Hardingham, D.J. Wyllie, S. Chandran, Physiological normoxia and absence of EGF is required for the long-term propagation of anterior neural precursors from human pluripotent cells, PLoS One 9 (1) (2014) e85932.
[54] D. Bridges, K. Fisher, S.N. Zolov, T. Xiong, K. Inoki, L.S. Weisman, A.R. Saltiel, Rab5 proteins regulate activation and localization of target of rapamycin complex 1, J. Biol. Chem. 287 (25) (2012) 20913–20921.
[55] J.M. Hyttinen, M. Niittykoski, A. Salminen, K. Kaarniranta, Maturation of autophagosomes and endosomes: a key role for Rab7, Biochim. Biophys. Acta 1833 (3) (2013) 503–510.
[56] J. Rappaport, R.L. Manthe, M. Solomon, C. Garnacho, S. Muro, A comparative study on the alterations of endocytic pathways in multiple lysosomal storage disorders, Mol. Pharm. 13 (2) (2016) 357–368.
[57] M. Cardone, C. Porto, A. Tarallo, M. Vicinanza, B. Rossi, E. Polishchuk, F. Donaudy, G. Andria, M.A. De Matteis, G. Parenti, Abnormal mannose-6-phosphate receptor trafficking impairs recombinant alpha-glucosidase uptake in Pompe disease fibroblasts, PathoGenetics 1 (1) (2008) 6.
[58] C. Spampanato, E. Feeney, L. Li, M. Cardone, J.A. Lim, F. Annunziata, H. Zare, R. Polishchuk, R. Puertollano, G. Parenti, et al., Transcription factor EB (TFEB) is a new therapeutic target for Pompe disease, EMBO Mol. Med. 5 (5) (2013) 691–706.
[59] D.L. Medina, A. Fraldi, V. Bouche, F. Annunziata, G. Mansueto, C. Spampanato, C. Puri, A. Pignata, J.A. Martina, M. Sardiello, et al., Transcriptional activation of lysosomal exocytosis promotes cellular clearance, Dev. Cell 21 (3) (2011) 421–430.
[60] V.K. Lund, K.L. Madsen, O. Kjaerulff, Drosophila Rab2 controls endosome-lysosome fusion and LAMP delivery to late endosomes, Autophagy 14 (9) (2018) 1520–1542.
[61] M.A. Samie, H. Xu, Lysosomal exocytosis and lipid storage disorders, J. Lipid Res. 55 (6) (2014) 995–1009.
[62] M. Sardiello, M. Palmieri, A. di Ronza, D.L. Medina, M. Valenza, V.A. Gennarino, C. Di Malta, F. Donaudy, V. Embrione, R.S. Polishchuk, et al., A gene network regulating lysosomal biogenesis and function, Science 325 (5939) (2009) 473–477.
[63] C. Settembre, C. Di Malta, V.A. Polito, M. Garcia Arencibia, F. Vetrini, S. Erdin, S.U. Erdin, T. Huynh, D. Medina, P. Colella, et al., TFEB links autophagy to lysosomal biogenesis, Science 332 (6036) (2011) 1429–1433.
[64] M.L. Schultz, L. Tecedor, M. Chang, B.L. Davidson, Clarifying lysosomal storage diseases, Trends Neurosci. 34 (8) (2011) 401–410.
[65] A. Biever, E. Valjent, E. Puighermanal, Ribosomal protein S6 phosphorylation in the nervous system: from regulation to function, Front. Mol. Neurosci. 8 (2015) 75.
[66] K. Kiselyov, S. Yamaguchi, C.W. Lyons, S. Muallem, Aberrant Ca2+ handling in lysosomal storage disorders, Cell Calcium 47 (2) (2010) 103–111.
[67] A. Raturi, T. Simmen, Where the endoplasmic reticulum and the mitochondrion tie the knot: the mitochondria-associated membrane (MAM), Biochim. Biophys. Acta 1833 (1) (2013) 213–224.
[68] M. Sandri, FOXOphagy path to inducing stress resistance and cell survival, Nat. Cell Biol. 14 (8) (2012) 786–788.
[69] A.M. Orogo, A.B. Gustafsson, Therapeutic targeting of autophagy: potential and concerns in treating cardiovascular disease, Circ. Res. 116 (3) (2015) 489–503.
[70] X. Chen, Y. He, F. Lu, Autophagy in stem cell biology: a perspective on stem cell self-renewal and differentiation, Stem Cell. Int. 2018 (2018) 9131397.
[71] I. Tanida, T. Ueno, E. Kominami, LC3 conjugation system in mammalian autophagy,

Int. J. Biochem. Cell Biol. 36 (12) (2004) 2503–2518.
[72] E. Seranova, K.J. Connolly, M. Zatyka, T.R. Rosenstock, T. Barrett, R.I. Tuxworth, S. Sarkar, Dysregulation of autophagy as a common mechanism in lysosomal storage diseases, Essays Biochem. 61 (6) (2017) 733–749.
[73] N. Mizushima, T. Yoshimori, How to interpret LC3 immunoblotting, Autophagy 3 (6) (2007) 542–545.
[74] M. Kadowaki, M.R. Karim, Cytosolic LC3 ratio as a quantitative index of macroautophagy, Methods Enzymol. 452 (2009) 199–213.
[75] N.W. Andrews, Membrane resealing mediated by lysosomal exocytosis, [Internet], Madame Curie Bioscience Database, Landes Bioscience, Austin (TX), 2000-2013.
[76] S. Vitry, J. Bruyere, M. Hocquemiller, S. Bigou, J. Ausseil, M.A. Colle, M.C. Prevost, J.M. Heard, Storage vesicles in neurons are related to Golgi complex alterations in mucopolysaccharidosis IIIB, Am. J. Pathol. 177 (6) (2010) 2984–2999.
[77] G.R. Villani, A. Chierchia, D. Di Napoli, P. Di Natale, Unfolded protein response is not activated in the mucopolysaccharidoses but protein disulfide isomerase 5 is deregulated, J. Inherit. Metab. Dis. 35 (3) (2012) 479–493.
[78] W. Li, J. Zhu, J. Dou, H. She, K. Tao, H. Xu, Q. Yang, Z. Mao, Phosphorylation of LAMP2A by p38 MAPK couples ER stress to chaperone-mediated autophagy, Nat. Commun. 8 (1) (2017) 1763.
[79] N. Sovolyova, S. Healy, A. Samali, S.E. Logue, Stressed to death - mechanisms of ER stress-induced cell death, Biol. Chem. 395 (1) (2014) 1–13.
[80] K. Nakamura, E. Bossy-Wetzel, K. Burns, M.P. Fadel, M. Lozyk, I.S. Goping, M. Opas, R.C. Bleackley, D.R. Green, M. Michalak, Changes in endoplasmic reticulum luminal environment affect cell sensitivity to apoptosis, J. Cell Biol. 150 (4) (2000) 731–740.
[81] M. Michalak, J. Groenendyk, E. Szabo, L.I. Gold, M. Opas, Calreticulin, a multiprocess calcium-buffering chaperone of the endoplasmic reticulum, Biochem. J. 417 (3) (2009) 651–666.
[82] J.P. Decuypere, G. Monaco, G. Bultynck, L. Missiaen, H. De Smedt, J.B. Parys, The IP(3) receptor-mitochondria connection in apoptosis and autophagy, Biochim. Biophys. Acta 1813 (5) (2011) 1003–1013.
[83] C. Dubois, F. Vanden Abeele, N. Prevarskaya, Targeting apoptosis by the remodelling of calcium-transporting proteins in cancerogenesis, FEBS J. 280 (21) (2013) 5500–5510.
[84] P. Li, L. Zhou, T. Zhao, X. Liu, P. Zhang, Y. Liu, X. Zheng, Q. Li, Caspase-9: structure, mechanisms and clinical application, Oncotarget 8 (14) (2017) 23996–24008.
[85] M.L. Wurstle, M.A. Laussmann, M. Rehm, The central role of initiator caspase-9 in apoptosis signal transduction and the regulation of its activation and activity on the apoptosome, Exp. Cell Res. 318 (11) (2012) 1213–1220.
[86] C. Di Malta, J.D. Fryer, C. Settembre, A. Ballabio, Astrocyte dysfunction triggers neurodegeneration in a lysosomal storage disorder, Proc. Natl. Acad. Sci. U.S.A. 109 (35) (2012) E2334–E2342.
[87] A. Chandrasekaran, H.X. Avci, M. Leist, J. Kobolak, A. Dinnyes, Astrocyte differentiation of human pluripotent stem cells: new tools for neurological disorder research, Front. Cell. Neurosci. 10 (2016) 215.
[88] K.V. Rama Rao, T. Kielian, Astrocytes and lysosomal storage diseases, Neuroscience 323 (2016) 195–206.
[89] R.E. Gale, H. Wheadon, P. Boulos, D.C. Linch, Tissue specificity of X-chromosome inactivation patterns, Blood 83 (10) (1994) 2899–2905.
[90] D. Elstein, E. Schachamorov, R. Beeri, G. Altarescu, X-inactivation in Fabry disease, Gene 505 (2) (2012) 266–268.
[91] D.P. Germain, L. Echevarria, Tissue-specific X chromosome inactivation studies as a decision-making criteria for enzyme replacement therapy in female heterozygotes for Fabry disease, Mol. Genet. Metabol. 111 (2) (2014) S45.
[92] L.L. de Camargo Pinto, S.W. Maluf, S. Leistner-Segal, C. Zimmer da Silva, A. Brusius-Facchin, M.G. Burin, S. Brustolin, J. Llerena, L. Moraes, L. Vedolin, et al., Are MPS II heterozygotes actually asymptomatic? A study based on clinical and biochemical data, X-inactivation analysis and imaging evaluations, Am. J. Med. Genet. 155A (1) (2011) 50–57.
[93] T. Tukiainen, A.C. Villani, A. Yen, M.A. Rivas, J.L. Marshall, R. Satija, M. Aguirre, L. Gauthier, M. Fleharty, A. Kirby, et al., Landscape of X chromosome inactivation across human tissues, Nature 550 (7675) (2017) 244–248.
[94] B. Papp, K. Plath, Epigenetics of reprogramming to induced pluripotency, Cell 152 (6) (2013) 1324–1343.
[95] N. Salomonis, P.J. Dexheimer, L. Omberg, R. Schroll, S. Bush, J. Huo, L. Schriml, S. Ho Sui, M. Keddache, C. Mayhew, et al., Integrated genomic analysis of diverse induced pluripotent stem cells from the progenitor cell biology consortium, Stem Cell. Rep. 7 (1) (2016) 110–125.